JOURNAL OF PETROLOGY | VOLUME 49 | NUMBER 10 | PAGES 1817–1852 | 2008 | doi:10.1093/petrology/egn048

Melt Depletion and Enrichment beneath the Western Kaapvaal Craton: Evidence from Finsch Peridotite Xenoliths

SALLY A. GIBSON*, JACQUELINE MALARKEY† AND JASON A. DAY

DEPARTMENT OF EARTH SCIENCES, UNIVERSITY OF CAMBRIDGE, DOWNING STREET, CAMBRIDGE CB2 3EQ, UK

RECEIVED DECEMBER 6, 2007; ACCEPTED SEPTEMBER 12, 2008
ADVANCE ACCESS PUBLICATION OCTOBER 22, 2008

We present major- and trace-element analyses of mineral phases present in a suite of 16 garnet-peridotite xenoliths from the western terrane of the Kaapvaal craton. The xenoliths were entrained by a Group II Finsch kimberlite at 118 Ma, shortly prior to a major metasomatic event that caused widespread enrichment of the Kaapvaal lithospheric mantle. Compositionally homogeneous grains of olivine, orthopyroxene, garnet and clinopyroxene and coarse–equant textures indicate equilibrium relationships between mineral phases in the majority of xenoliths. Pressure and temperature estimates suggest that clinopyroxene-bearing garnet peridotites last equilibrated at 1130–1270°C and 45–59 kbar whereas clinopyroxene-free xenoliths record temperatures of 1000–1070°C and pressures of 34–42 kbar. The Finsch xenoliths plot on a conductive palaeogeotherm with a surface heat flux of ~46 mW m^2. Combined Ca and Cr abundances of Finsch pyrope garnets suggest that both lherzolitic and harzburgitic parageneses are present. Samples bearing sub-calcic (harzburgitic) garnets are from the shallowest depths. The lherzolitic garnets are depleted in light rare earth elements (LREE) relative to the middle and heavy REE (MREE and HREE) and have 'smooth' chondrite-normalized patterns. In contrast, the sub-calcic garnets are characterized by sinusoidal chondrite-normalized REE patterns that peak at Nd and Lu and exhibit lows at La and Er. The sub-calcic garnets also have lower Zr, Hf, Ti and HREE, and higher LREE and Sr, than lherzolitic garnets. The variations in REE ratios correlate with temperature and pressure and also Cr/Ca ratio. The high Cr content of harzburgitic and some lherzolitic Finsch garnets may have a significant effect on the crystal framework. Substitution of the larger Cr^{3+} ion for the smaller Al^{3+} ion increases with decreasing temperature and pressure and distorts the crystal lattice; this permits a greater substitution of Ca by large cations, such as Sr and the LREE, but also limits the replacement of Al by Ti, Zr and Hf. Positive HREE slopes displayed by harzburgitic garnets on chondrite-normalized plots are believed to result from metasomatic enrichment by a melt that had already undergone significant garnet fractionation during ascent through the lithospheric mantle. The low-temperature Finsch peridotites are characterized by much lower orthopyroxene (<17%) and higher olivine (up to 96%) modal abundances than have been reported from xenolith suites elsewhere in the Kaapvaal craton. Significantly, they resemble residues generated in partial melting experiments. The Finsch harzburgites have very low Al_2O_3 (0·18 wt %) and CaO (0·38 wt %) and high MgO contents (49·75 wt %) and appear to be highly refractory. They also have high bulk-rock Mg/(Mg + Fe) and high modal olivine contents, and in this respect resemble some of those recently described from NW Canada and Greenland. We suggest that some of the Finsch low-temperature peridotites represent Kaapvaal lithospheric mantle that formed as a residue of adiabatic decompression melting between 4·5 and 1·5 GPa. The inferred mantle potential temperature of 1550°C would have been similar to that of ambient Archaean mantle. Importantly, it appears that the sub-Finsch lithospheric mantle has remained unmodified by the silica enrichment that has been so prevalent elsewhere in the craton. This may reflect the remoteness from the subduction zone that is believed to have been in existence at 2·9 Ga on the eastern margin of the craton.

KEY WORDS: *Kaapvaal craton; peridotite; harzburgite; mantle enrichment, melt depletion*

INTRODUCTION

Mantle xenoliths provide a unique insight into the composition of the Earth's deep interior and invaluable

*Corresponding author Telephone: +44 1223 333400. Fax: +44 1223 333450. E-mail: sally@esc.cam.ac.uk
†Present address: Department of Earth Sciences, Durham University, Science Labs, Durham DH1 3LE, UK.

information on the thermal structure of the lithosphere. They also offer an opportunity to constrain the melt depletion and enrichment processes that have been involved in the evolution of the Earth's subcontinental lithospheric mantle from Archaean to Recent times. Many mantle xenoliths have, however, undergone extensive modification since the time of their formation such that mineralogical and geochemical evidence relating to processes involved in the very early stages of lithosphere formation is overprinted. For example, kimberlites from all of the major cratons have entrained peridotite xenoliths that have experienced mantle metasomatism (e.g. Dawson & Smith, 1977, 1988; Harte *et al.*, 1987; Pearson *et al.*, 1995*a*; Kopylova & Caro, 2004). This is widely believed to have resulted from percolation of small-fraction volatile-rich melts derived from the convecting mantle. Sometimes metasomatism is evident from the growth of 'new' phases such as garnet, clinopyroxene and/or phlogopite but in other cases only the mineral chemistry has changed. The latter, 'cryptic' metasomatism (Dawson, 1984), is especially apparent in incompatible trace element concentrations and ratios. Studies of pyrope garnets have shown that those belonging to the harzburgite paragenesis (i.e. low Ca and often high Cr), and believed to represent depleted mantle, are characterized by sinusoidal chondrite-normalized rare earth element (REE) patterns with a peak at Nd or Sm and sometimes Lu. In contrast, lherzolitic garnets, thought to typify fertile or metasomatized mantle, have smooth chondrite-normalized REE patterns with a positive slope for the light to middle REE (LREE to MREE) and a fairly flat MREE to heavy REE (HREE) slope. Furthermore, the low-Ca harzburgitic garnets usually have higher LREE concentrations than the lherzolitic garnets, which are often more Ca-rich. This paradox between the major element and REE concentrations of mantle garnets has provoked much discussion in the recent literature (e.g. Stachel *et al.*, 1998; Griffin *et al.*, 1999*a*; Wang *et al.*, 2000; Bell *et al.*, 2005). Although invoking a wide array of processes to explain the variations in REE, most interpretations suggest that the source of the sub-calcic garnets has undergone metasomatism. If this is correct then much of the subcratonic lithospheric mantle has been modified by metasomatic enrichment since the time of its formation. Indeed, trace-element and isotopic ratios of peridotitic diamond inclusions suggest that enrichment of cratonic lithospheric mantle may have been operational since at least ~3·3 Ga (Richardson *et al.*, 1984; Pearson *et al.*, 1995*b*).

Incompatible trace-element enrichment of mantle xenoliths is also thought to occur as a result of the percolation of melts associated with the host kimberlite (Kinny & Dawson, 1992). Diffusion of both major and trace elements through grains in mantle xenoliths is significantly slower (hundreds of years; e.g. Van Orman *et al.*, 2002) than the timescale of kimberlite emplacement (days; Kelley & Wartho, 2000) and this type of enrichment, immediately prior to or during ascent, results in compositionally heterogeneous grains. This is a common characteristic of peridotite xenoliths entrained by Group I South African kimberlites (e.g. Griffin *et al.*, 1999*c*; Simon *et al.*, 2003; Burgess & Harte, 2004). As well as overprinting the original mantle 'signature', chemical disequilibrium within and between grains considerably restricts the application of geothermometers and barometers.

A different style of metasomatism, involving SiO_2-enriched fluids and/or melts, has been attributed by some to low-temperature (<1150°C) peridotite xenoliths from the Kaapvaal and Siberian cratons. The orthopyroxene contents and Si/Mg ratios of these xenoliths are higher than those of residues generated in partial melting experiments (e.g. Boyd, 1989). Recent studies have reinstated the proposal of Kesson & Ringwood (1989) that the silica enrichment results from the invasion of cratonic lithosphere by hydrous fluids and/or melts derived from a subducting slab (Rudnick *et al.*, 1994; Kelemen *et al.*, 1998; Bell *et al.*, 2005; Simon *et al.*, 2007). This contrasts with models which suggest that the ubiquitous high modal orthopyroxene in low-temperature peridotites from the Kaapvaal and Siberian cratons resulted from high-pressure melting processes that occurred at the time of lithosphere formation (Boyd, 1989; Herzberg, 1999).

In this study we report on a suite of peridotite xenoliths entrained by the Finsch kimberlite from beneath the western part of the Kaapvaal craton. The Finsch peridotites are of particular interest because: (1) they display a continuum of compositions ranging from harzburgites to lherzolites; (2) unlike most peridotites from other parts of the craton, all of the mineral phases are in chemical equilibrium; (3) the modal abundance of orthopyroxene in the low-temperature peridotites is much less than previously described from locations further east in the Kaapvaal craton. It is, however, similar to that reported in recent studies of xenoliths from Greenland and NW Canada (e.g. Bernstein *et al.*, 1998; Schmidberger & Francis, 1999). We have combined our new petrographic and geochemical results with those previously described for 3·3 Ga Finsch peridotitic diamond inclusions (Richardson *et al.*, 1984) and xenoliths (Gurney & Switzer, 1973; Shee *et al.*, 1982; Skinner, 1989; Viljoen *et al.*, 1992) to gain further understanding of the long-term lithospheric mantle evolution of the Kaapvaal craton. Our detailed petrological and geochemical study of all phases present in the Finsch xenolith suite complements recent work on the Kaapvaal craton that has focused on specific mineral phases, such as pyrope garnet (e.g. Griffin *et al.*, 1999*b*; Burgess & Harte, 2004).

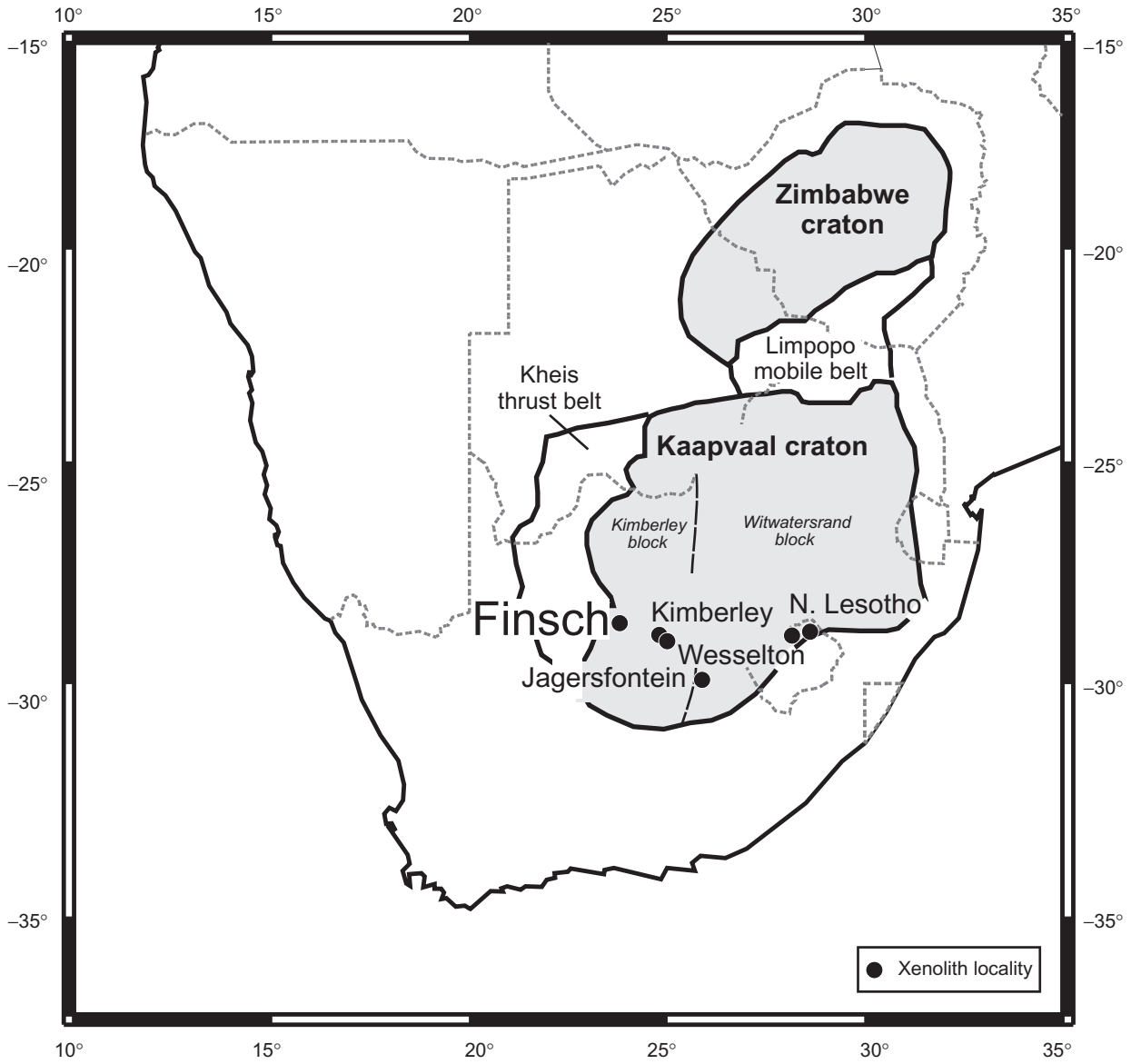

Fig. 1. Location of the Finsch kimberlite cluster and on the western margin of the Kaapvaal craton, together with other xenoliths mentioned in the text. Seismic boundaries of the Kaapvaal craton and adjacent tectonic units are from Fouch *et al.* (2004) and Schmitz *et al.* (2004).

GEOLOGICAL SETTING AND PREVIOUS INVESTIGATIONS OF FINSCH PERIDOTITES

The Finsch kimberlite cluster is located at 28°21'S, 23°28'E, on the western margin of the Kimberley Block (Fig. 1). It represents one of the westernmost kimberlite localities described from the Kaapvaal craton. Kimberlite was first identified in 1960 and diamond production at Finsch Mine has been in operation since 1964. Fresh peridotite xenoliths were not, however, discovered until the late 1970s. Detailed mapping has revealed the presence of three kimberlite pipes and three dykes (Ekkerd *et al.*, 2003). These intrude the Karoo and Griqualand West Groups. Erosion has removed the Karoo sediments and the upper, crater-facies parts of the pipes and exposed hypabyssal-facies kimberlites. The F1 kimberlite is the dominant intrusion but the rare mantle xenoliths (peridotites and eclogites) were found in a small intrusion of melilite-rich phlogopite kimberlite (F7) and a kimberlite breccia (F8), which represents the highest-grade ore-body at Finsch Mine (Ekkerd *et al.*, 2003).

In terms of their petrography and bulk-rock chemistry, the Finsch kimberlites resemble other Group II southern African kimberlites (Fraser & Hawkesworth, 1992). Rb–Sr phlogopite ages suggest that Finsch was emplaced at 118·4 ± 2·2 Ma, at a similar time to other Group II southern African kimberlites; for example, those from Barkley West and Boshof (Smith *et al.*, 1985).

Combined petrographic descriptions and analyses of major-element mineral chemistry are available in the published literature for 15 garnet peridotites and a garnet websterite (Gurney & Switzer, 1973; Shee *et al.*, 1982; Smith *et al.*, 1985; Skinner, 1989; Viljoen *et al.*, 1992). Radiogenic isotope determinations have also been made on a small number of peridotite xenoliths (Pearson *et al.*, 1995*a*; Griffin *et al.*, 2004). In addition, geochemical studies have been undertaken on the Finsch kimberlite concentrate (Gurney & Switzer, 1973) and on peridotite and eclogite diamond-inclusion suites (Gurney *et al.*, 1979; Richardson *et al.*, 1984; Shimizu & Richardson, 1987; Smith *et al.*, 1991; Griffin *et al.*, 1992; Appleyard *et al.*, 2004).

At least four of the peridotite xenoliths previously described from Finsch are known to be diamondiferous (Shee *et al.*, 1982; Viljoen *et al.*, 1992). These, together with those reported from Roberts Victor (Viljoen *et al.*, 1994) and Udachnaya (Sobolev *et al.*, 1984), are amongst the largest known number of samples of diamondiferous peridotites from a single locality for which there is information available in international published literature. Sm–Nd model ages suggest that sub-calcic pyrope garnet inclusions in Finsch diamonds formed at ~3·3 Ga (Richardson *et al.*, 1984). Furthermore, the incompatible trace element and Sm–Nd isotopic ratios of these garnets indicate that, prior to diamond formation, the mantle had undergone both melt depletion and enrichment events (Richardson *et al.*, 1984; Shimizu & Richardson, 1987). Re–Os ratios for both whole-rock samples and sulphides in Finsch peridotites confirm that a melt depletion event occurred prior to ~3 Ga (Pearson *et al.*, 1995*a*; Griffin *et al.*, 2004). Considerably higher and varied Nd isotopic ratios for garnets from the Finsch peridotites, relative to those in the diamond inclusions (Richardson *et al.*, 1984; Shimizu & Richardson, 1987; Pearson *et al.*, 1995*a*), suggest that lithospheric enrichment may have continued until immediately prior to their entrainment.

PETROGRAPHY

We have studied a total of 16 peridotite xenoliths from Finsch Mine. Six of these were collected by J. B. Dawson from the F7 intrusion, exposed in the open pit in 1979 (sample numbers with the prefix BD), and the remainder were collected by J. Malarkey (F05JM sample numbers) during a visit to the mine in 2005. The xenoliths are rounded to ellipsoidal in shape and reach >50 cm in diameter. They exhibit variable degrees of alteration. Most xenoliths have a weathered outer surface but a relatively fresh interior, and petrographically fresh material was obtained in all but two cases (F05JM1 and BD3697A). In the latter, olivine has been completely serpentinized but the other phases are generally fresh. In the majority of the xenoliths, alteration is restricted to cracks in olivine grains.

The Finsch mantle xenolith suite is dominated by clinopyroxene-bearing garnet peridotites. Estimates of modal mineralogy were made using image analysis software (ImageJ©) on both thin sections and hand specimens. The results are shown in Table 1. Both olivine and orthopyroxene exhibit large variations in modal abundances, varying from 60 to 96 modal % and from 1 to 33%, respectively. Small modal amounts of garnet (1–8%) and clinopyroxene (0–5%) are also present. Phlogopite is rare and tends to be restricted to the margins of kelyphitic rims that surround garnet, or as a replacement for clinopyroxene. The variations in modal mineralogy that we have observed are similar to those reported in previous studies of Finsch xenoliths (Table 1; Shee *et al.*, 1982; Skinner, 1989).

The most abundant textural type of mantle xenoliths at Finsch are coarse–tabular peridotites (based on the definitions of Harte, 1977). This texture is displayed by all of the clinopyroxene-bearing xenoliths and is defined by tabular grains of olivine and orthopyroxene that have straight grain boundaries. Olivine forms 67–89 modal % of these rocks and is up to 14 mm in diameter. Orthopyroxene contents vary between 7 and 33 modal %. The orthopyroxene grains are up to 6 mm in diameter and exhibit undulose extinction. Garnet forms 3·5–8·3 modal % of the coarse–tabular peridotites. The grains are red in hand specimen and pink in thin section, rounded and are commonly 3–4 mm in diameter, although a few reach up to 1 cm (Supplementary Images are available for downloading at http://petrology.oxfordjournals.org). The garnets show no evidence of recrystallization or shearing but usually have thin kelyphitic rims. In the coarse–tabular peridotites, clinopyroxene occurs as small (<3 mm), anhedral (often lobate), emerald green, strain-free grains and constitutes 1–4·7 modal % of the rock. The clinopyroxenes often have narrow (~200 μm) 'spongy' corroded rims. In F05JM6, the clinopyroxenes have well-developed exsolution lamellae that are truncated by the 'spongy' rims. SEM back-scattered images and qualitative spectra analyses suggest that the rims and cores have the same composition; this indicates that the corroded rims are probably the result of partial melting of the clinopyroxene, perhaps during kimberlite emplacement. Only one sample (F05JM2) displays evidence of recrystallization of olivine to strain-free neoblasts and has extensively strained orthopyroxene (i.e. has a porphyroclastic texture). Neither the garnet nor clinopyroxene show evidence of recrystallization in this sample.

Table 1: Summary of petrography and classification of Finsch mantle xenoliths

	Distinguishing petrographic characteristics			Modal abundance					Garnet paragenesis
	Texture	Garnet appearance	Phlogopite	Olivine	Opx	Cpx	Garnet	Phlogopite	from Ca vs Cr plot
BD3692	Coarse-tabular	Fresh, red	Replacing cpx	76·71	16·51	3·14	3·64	Trace	Low-Cr lherzolite
BD3693	Coarse-tabular	Fresh, red	Replacing cpx	71·73	19·75	4·25	4·27	Trace	Low-Cr lherzolite
BD3697A	Coarse-tabular	Fresh, red	Replacing cpx	67·38	23·53	3·68	5·41	Trace	Low-Cr lherzolite
BD3697B	Coarse-tabular	Fresh, red	—	75·33	19·08	1·83	3·76	—	Low-Cr lherzolite
BD3692	Coarse-tabular	Fresh, red	Replacing cpx	67·91	25·31	3·14	3·64	Trace	Low-Cr lherzolite
JM1	Coarse-tabular	Fresh, red	—	88·62	6·94	0·86	3·58	—	Low-Cr lherzolite
JM2	Porphyroclastic	Fresh, red	Replacing cpx	79·45	10·09	2·19	8·27	Trace	Low-Cr lherzolite
JM3	Coarse-tabular	Fresh, red	Around gt rim	88·87	6·41	—	4·72	Trace	Low-Cr lherzolite
JM4	Coarse-tabular	Fresh, red	—	60·17	33·24	1·27	5·32	—	Low-Cr lherzolite
JM6	Coarse-tabular	Fresh, red	Replacing cpx	78·45	10·94	4·71	5·90	Trace	Low-Cr lherzolite
JM7	Coarse-tabular	Fresh, red	—	81·43	14·10	0·95	3·52	—	Low-Cr lherzolite
JM10	Coarse-tabular	Fresh, red	Replacing cpx	83·93	9·13	2·52	4·41	Trace	Low-Cr lherzolite
BD3694	Coarse-equant	Partially fresh, lilac	—	80·15	17·70	—	2·15	—	High-Cr Lherzolite
BD3695	Coarse-equant	Partially fresh, lilac	In vein	96·05	2·0	—	1·95	Trace	High-Cr Lherzolite
JM8	Coarse-equant	Partially fresh, lilac	—	82·78	14·39	—	2·83	—	High-Cr Lherzolite
JM5	Coarse-equant	Partially altered, lilac	—	95·08	0·90	—	4·01	—	Dunite
JM9	Coarse-equant	Partially altered, lilac	—	92·42	6·66	—	0·91	—	Harzburgite

Clinopyroxene-free xenoliths (F05JM5, 8 and 9; BD3694 and 3695) have coarse–equant textures. These xenoliths are very rich in olivine (80–96 modal %, Table 1) and have variable amounts of orthopyroxene (2–18 modal %) and low amounts of garnet (1–4 modal %). The olivine grains have straight or smoothly curving grain boundaries and are up to 12 mm in length. They often display 120° triple junctions with orthopyroxene and appear to be in textural equilibrium. They exhibit slight undulose extinction. Orthopyroxene has diameters up to 5 mm. Garnet is relatively evenly distributed through the coarse–equant xenoliths. Grains are generally anhedral and range in size from 4 to 10 mm. They have thick kelyphitic rims of spinel and phlogopite and are readily distinguished from garnets in the coarse–tabular peridotites by their lilac colour and partially altered appearance (see Supplementary Images).

MINERAL CHEMISTRY

The major- and trace-element systematics of mantle phases are highly dependent upon bulk-rock assemblages as well as temperature and pressure. In harzburgites, garnet is the major host of the REE, Sc, Y, Ti, Zr, Sr, Nb and Hf whereas in lherzolites these trace elements are partitioned between both garnet and clinopyroxene. Below we summarize variations in the major- and trace-element concentrations of single phases and then consider the implications of these to our understanding of mantle processes. Representative analyses of mineral phases are shown in Table 2 and in the Supplementary Dataset (http://petrology.oxfordjournals.org/).

ANALYTICAL TECHNIQUES

Olivine, orthopyroxene, clinopyroxene and garnet were analysed for major and some trace elements using a Cameca SX100 electronprobe microanalyser equipped with five wavelength-dispersive spectrometers at the University of Cambridge. Both rim and core measurements were taken for the garnets as well as a traverse across one garnet in each section. During each analysis the beam voltage was 15 kV and the beam diameter was 1 μm. A current of 10 nA was employed for major elements and 100 nA for trace elements. The peak counting time was 20 s and background time half this. Standards were natural silicates, pure oxides and metals. Details of detection limits are given in the Supplementary Dataset.

Trace-element concentrations (Hf, Nb, Pb, Sc, Sr, Ta, Th, U, REE) in clinopyroxene and garnet were determined using a New Wave UP213 Nd:YAG laser ablation system interfaced to a Perkin–Elmer Elan DRC II inductively coupled plasma mass spectrometer (ICP-MS) system at the University of Cambridge. The diameter of the laser beam was 120 μm, the laser repetition rate was 10 Hz and the laser power was ~12 J/cm. The ICP-MS data acquisition settings were two sweeps per reading,

Table 2: Representative mineral analyses

Lithology:	Clinopyroxene Lherzolite													
Sample no.:	F05JM1	F05JM1	F05JM2	F05JM6	F05JM6	F05JM7	F05JM7	F05JM7	BD3692	BD3693	BD3693	BD3697A	F05JM10	F05JM3
Grain:	CPX2	CPX1C1	CPX3R1	CPX1C1	CPX3R1	CPX1	CPX2	CPX4	CPX2	CPX10C1	CPX3C1	CPX2C2	CPX4	CPX1
Location in grain:		core	rim	core	rim					core	core	core		
Major elements (wt%)														
SiO_2	55·01	55·44	54·76	55·26	55·34	55·26	55·24	54·98	55·65	55·26	55·30	55·26	54·77	55·14
TiO_2	0·05	0·14	0·15	0·07	0·07	0·09	0·12	0·11	0·17	0·16	0·17	0·17	0·16	0·11
Al_2O_3	1·49	1·93	1·97	1·79	1·79	1·77	1·78	1·78	2·91	2·94	2·94	2·91	0·67	1·88
Cr_2O_3	1·67	1·29	1·31	1·27	1·25	1·47	1·55	1·47	1·77	1·79	1·83	1·79	1·88	1·93
FeO	2·27	2·81	2·86	2·51	2·52	2·57	2·77	2·72	2·39	2·39	2·35	2·34	2·39	2·42
MnO	0·08	0·10	0·10	0·09	0·10	0·10	0·11	0·11	0·08	0·10	0·08	0·07	0·10	0·09
MgO	18·13	17·85	17·69	17·89	17·92	17·76	17·76	17·84	16·33	16·47	16·42	16·54	18·12	17·72
NiO	0·05	0·05	0·07	0·06	0·07	0·07	0·04	0·05	0·05	0·05	0·06	0·04	0·05	0·05
CaO	19·45	18·67	18·65	19·24	19·34	18·68	18·67	18·91	18·32	18·14	18·14	18·21	20·46	18·31
Na_2O	1·39	1·71	1·71	1·46	1·49	1·58	1·66	1·67	2·41	2·51	2·56	2·44	0·89	1·84
K_2O	0·09	0·03	0·04	0·08	0·08	0·09	0·10	0·10	0·04	0·04	0·04	0·05	0·00	0·04
Total	99·68	100·03	99·30	99·72	99·97	99·42	99·79	99·75	100·09	99·83	99·89	99·81	99·49	99·53
Trace elements (ppm)														
Ba	0·63	0·30	0·31		1·20	1·64	2·08	1·80	1·04	0·54	0·71			
Ga	2·61	3·96	4·34		3·79	3·80	3·56	3·93	5·37	4·05	3·80			
Hf	0·14	0·18	0·16			0·67	0·91	0·80	0·52	0·51	0·54			
Nb	0·48	0·26	0·28		0·57	0·15	0·14	0·15	0·74	0·75	0·63			
Ni	383	433	461		424	413	417	417	382	233	230			
Pb	0·43								0·82					
Sc	13·93	17·16	16·79		12·23	13·66	14·14	13·99	18·00	13·83	13·57			
Rb	0·02	<0·023	0·02		0·10	0·03	0·03	0·03	0·07	0·01	0·02			
Sr	83·6	76·2	73·8		59·7	147	164	165	149	122	114			
Th	0·03	0·03	0·02			0·04	0·05	0·04	0·11	0·10	0·12			
Ti	317	847	834			670	673	666	883	775	761			
U	0·00	0·01	0·01			0·02	0·01	0·01	0·03	0·03	0·02			
Y	0·46	1·26	1·10		1·09	1·51	2·02	1·83	2·17	2·06	2·06			
Zr	1·99	3·00	3·15		1·71	15·69	15·84	14·98	8·54	8·47	8·20			
La	2·33	1·35	1·27		3·70	4·00	4·15	3·89	7·02	7·60	7·23			
Ce	6·65	4·76	4·85		10·87	16·40	17·01	16·20	21·94	21·24	21·17			
Pr	0·98	0·71	0·73		1·08	2·29	2·36	2·18	2·50	2·45	2·38			
Nd	4·14	3·82	3·58		3·68	9·22	10·48	9·00	8·75	8·10	7·75			
Sm	0·49	0·93	0·91		0·65	1·42	1·72	1·56	1·44	1·32	1·44			
Eu	0·12	0·31	0·31		0·18	0·37	0·46	0·41	0·44	0·44	0·43			
Gd	0·32	0·70	0·81		0·55	1·08	1·26	1·04	1·40	1·30	1·20			
Tb	0·03	0·08	0·09		0·06	0·11	0·12	0·10	0·14	0·13	0·14			
Dy	0·12	0·35	0·32		0·26	0·42	0·59	0·51	0·65	0·61	0·64			
Ho	0·02	0·06	0·04		0·04	0·07	0·08	0·07	0·08	0·08	0·10			
Er	0·04	0·11	0·09		0·10	0·12	0·16	0·15	0·18	0·18	0·17			
Tm	0·00	0·01	0·01		0·01	0·01	0·02	0·02	0·02	0·02	0·02			
Yb	0·03	0·08	0·06		0·04	0·07	0·08	0·08	0·08	0·08	0·10			
Lu	0·01	0·01	0·01		0·01	0·01	0·01	0·02	0·01	0·01	0·01			

(continued)

Table 2: Continued

	Orthopyroxene													
Lithology:	Lherzolite												Dunite	Harzburgite
Sample:	F05JM1	F05JM2	F05JM3	F05JM4	F05JM6	F05JM7	F05JM8	F05JM10	BD3692	BD3693	BD3694	BD3697B	F05JM5	F05JM9
Grain:	OPX1	OPX4C2	OPX5	OPX2C2	OPX5	OPX9	OPX3	OPX2PT1	2OPX2	OPX4C2	OPX5	OPX4	OPX3	OPX3
Location in grain:		core		core										
Major elements (wt%)														
SiO_2	58·03	57·87	58·25	58·10	58·45	58·00	58·47	58·15	57·97	57·90	58·36	58·18	58·26	58·03
TiO_2	0·03	0·08	0·05	0·03	0·04	0·04	0·03	0·08	0·07	0·05	0·01	0·03	0·04	0·04
Al_2O_3	0·55	0·65	0·62	0·56	0·60	0·57	0·51	0·61	0·67	0·67	0·52	0·59	0·48	0·56
Cr_2O_3	0·33	0·26	0·37	0·33	0·23	0·26	0·38	0·30	0·24	0·24	0·35	0·32	0·54	0·53
FeO	4·63	5·22	4·66	5·01	4·89	5·18	4·14	4·91	4·80	4·76	4·30	4·52	4·97	4·32
MnO	0·10	0·14	0·10	0·12	0·12	0·13	0·11	0·09	0·11	0·12	0·13	0·10	0·13	0·11
MgO	35·21	34·62	35·06	35·13	34·75	34·95	35·55	34·93	35·34	35·68	35·42	35·34	35·14	35·87
NiO	0·12	0·12	0·12	0·10	0·14	0·11	0·12	0·12	0·13	0·12	0·12	0·12	0·12	0·13
CaO	0·71	0·71	0·66	0·68	0·69	0·70	0·66	0·66	0·52	0·52	0·67	0·66	0·73	0·36
Na_2O	0·15	0·17	0·18	0·12	0·15	0·17	0·10	0·19	0·17	0·19	0·09	0·13	0·17	0·11
Total	99·86	99·84	100·07	100·17	100·06	100·11	100·05	100·03	100·02	100·25	99·98	100·00	100·58	100·07

	Olivine												
Lithology:	Lherzolite											Dunite	Harzburgite
Sample:	F05JM2	F05JM3	F05JM4	F05JM6	F05JM7	F05JM8	F05JM10	BD3692	BD3693	BD3694	BD3695	F05JM5	F05JM9
Grain:	OI1	OL1	OL1	OL5	OL3	OL9	OL5	OL2	OI1C1	OL1	BD5OL1	FJM5OL7	FJM9OL10
Major elements (wt%)													
SiO_2	41·63	41·38	41·44	41·37	41·20	41·73	41·42	41·34	41·41	40·97	41·42	41·26	41·50
TiO_2	0·01	0·01	0·01	0·01	0·01	0·01	0·01	0·01	0·00	0·00	0·02	0·00	0·02
Al_2O_3	0·01	0·01	0·01	0·01	0·01	0·01	0·01	0·01	0·01	0·01	0·01	0·01	0·01
Cr_2O_3	0·02	0·04	0·01	0·04	0·03	0·05	0·03	0·04	0·03	0·05	0·05	0·08	0·04
FeO	8·87	7·65	7·90	8·30	8·34	7·02	8·11	7·85	8·03	7·65	7·53	8·20	7·30
MnO	0·11	0·11	0·08	0·09	0·11	0·11	0·12	0·08	0·09	0·09	0·08	0·11	0·09
MgO	49·12	50·11	50·00	49·73	49·89	50·64	49·88	50·42	50·56	50·87	50·36	49·77	50·65
NiO	0·38	0·38	0·36	0·41	0·39	0·39	0·43	0·44	0·42	0·40	0·36	0·41	0·41
CaO	0·04	0·04	0·05	0·04	0·04	0·05	0·03	0·03	0·02	0·03	0·04	0·04	0·02
Na_2O	0·02	0·03	0·01	0·01	0·02	0·01	0·03	0·02	0·02	0·03	0·03	0·02	0·02
Total	100·22	99·75	99·88	100·01	100·05	100·02	100·06	100·25	100·61	100·11	99·90	99·90	100·06

(continued)

40 readings, one replicate. The dwell times for each mass were dependent on the isotope and concentration of the element in the samples but was typically 10–50 ms. For all data, NIST 610 was used for calibration of element sensitivity. Calibration accuracy was verified by analysing either NIST 612 or 614 and MPIDING standards as unknown samples (see Supplementary Dataset); recoveries were typically 90–110% of the values published by Pearce *et al.* (1997) and Jochum (2006). The CaO content of each garnet and clinopyroxene was used for internal standard normalization of the trace-element signals. ICP-MS drift during the analytical session was less than 10%. The data were processed, and concentrations calculated, using Glitter Software (GEMOC, Australia) which allows precise selection of blanks, signals, and visualization of data quality.

Table 2: Continued

Lithology:	Garnet Lherzolite											
Sample:	F05JM1	F05JM1	F05JM2	F05JM2	F05JM3	F05JM3	F05JM4	F05JM4	F05JM6	F05JM6	F05JM7	F05JM7
Grain:		1Gt3C2	2Gt1C1	2Gt2R1	3GT1C2	3GT2C1	4GT3C1	4GT3R1	6GT2C1	6GT3R2	7GT1C1	7GT1R3
Location in grain	rim	core	core	rim	core	core	core	rim	core	rim	core	rim
Major elements (wt%)												
SiO_2	42·02	42·33	42·44	41·64	41·89	42·11	41·94	41·95	42·25	42·43	41·67	41·89
TiO_2	0·23	0·22	0·41	0·41	0·32	0·31	0·17	0·18	0·21	0·22	0·29	0·28
Al_2O_3	18·55	18·42	20·39	20·26	18·84	18·58	18·99	18·81	20·49	20·56	19·31	19·52
Cr_2O_3	6·46	6·55	3·69	3·78	6·09	6·03	5·78	6·16	3·69	3·86	5·25	5·01
FeO	6·56	6·61	7·49	7·47	6·64	6·65	6·85	6·82	6·97	6·96	7·20	7·23
MnO	0·33	0·29	0·32	0·33	0·32	0·30	0·33	0·32	0·29	0·32	0·32	0·32
MgO	20·55	20·49	20·47	20·41	20·69	20·54	20·55	20·28	20·83	21·16	20·91	20·87
CaO	5·48	5·44	4·75	4·75	5·22	5·18	5·37	5·44	4·70	4·77	5·10	5·02
Na_2O	0·04	0·02	0·07	0·06	0·04	0·06	0·03	0·03	0·03	0·03	0·04	0·04
P_2O_5	0·02	0·02	0·02	0·02	0·03	0·03	0·02	0·03	0·02	0·02	0·02	0·03
Total	100·24	100·38	100·05	99·11	100·10	99·80	100·04	100·02	99·48	100·33	100·12	100·21
Trace elements (ppm)												
Ba	0·04	<0·00	0·02	<0·00	0·05	<0·00	0·02	0·02	0·02	<0·00	0·03	0·02
Ga	6·80	6·54	8·68	9·26	6·54	6·67	6·99	6·97	8·65	8·98	9·87	9·62
Hf	0·54	0·55	0·49	0·45	0·82	0·78	1·09	1·15	0·44	0·45	0·29	0·31
Nb	1·04	1·02	0·36	0·37	0·35	0·35	0·53	0·48	0·78	0·88	0·99	0·82
Ni	60·18	58·13	74·63	77·85	56·30	55·54	67·36	66·87	67·12	62·09	71·71	64·91
Pb												
Rb	0·01	<0·016	0·01	0·01	<0·013	0·01	<0·032	<0·024	0·01	<0·041	0·00	<0·025
Sc	103·53	105·10	99·79	97·19	84·47	85·94	103·15	107·03	88·93	87·95	93·18	95·60
Sr	0·26	0·25	0·23	0·06	0·31	0·27	0·55	0·43	0·17	0·24	<0·210	0·16
Ta												
Th	0·04	0·02	0·01	0·03	0·01	0·03	0·03	0·02	0·04	0·02	0·04	0·06
U	0·04	0·05	0·01	0·03	0·02	0·01	0·03	0·03	0·03	0·04	0·09	0·07
Y	4·95	4·66	10·44	10·15	9·81	10·08	4·05	4·10	10·32	10·43	6·82	8·09
Zr	22·37	21·55	20·62	19·89	36·40	37·54	50·26	50·23	16·61	17·95	10·54	11·67
La	0·03	0·04	0·01	0·02	0·01	0·02	0·02	0·03	0·03	0·03	0·03	0·04
Ce	0·36	0·36	0·15	0·17	0·26	0·25	0·41	0·40	0·32	0·27	0·38	0·42
Pr	0·11	0·11	0·05	0·04	0·08	0·08	0·13	0·15	0·07	0·08	0·10	0·09
Nd	0·88	0·91	0·45	0·55	0·78	0·84	1·16	1·12	0·60	0·56	0·77	0·64
Sm	0·41	0·39	0·59	0·56	0·63	0·65	0·63	0·65	0·36	0·45	0·41	0·51
Eu	0·16	0·16	0·29	0·29	0·32	0·34	0·31	0·30	0·18	0·19	0·20	0·23
Gd	0·56	0·54	1·06	1·06	1·15	1·37	0·88	0·91	0·78	0·77	0·80	0·91
Tb	0·11	0·09	0·22	0·23	0·22	0·23	0·15	0·16	0·17	0·18	0·16	0·18
Dy	0·78	0·79	6·75	1·78	1·68	1·79	3·89	3·72	6·28	5·79	5·35	5·90
Ho	0·19	0·16	7·14	0·38	0·37	0·37	3·00	3·19	7·07	6·96	4·71	5·60
Er	0·57	0·49	7·51	1·18	1·07	1·12	2·34	2·90	8·21	7·54	5·08	5·38
Tm	0·10	0·09	8·02	0·19	0·17	0·18	2·32	2·72	9·07	9·35	4·05	4·89
Yb	0·85	0·85	8·61	1·28	1·24	1·27	2·52	3·37	9·88	9·69	5·71	6·74
Lu	0·16	0·12	9·31	0·22	0·20	0·21	3·26	3·79	10·69	11·14	5·89	6·91

(continued)

Table 2: Continued

Lithology:	Garnet Lherzolite											
Sample:	F05JM8	F05JM8	F05JM10	F05JM10	BD3692	BD3692	BD3693	BD3693	BD3694	BD3694	BD3695	BD3695
Grain:	8GT4C1	8GT4R1	10GT3C2	10GT3R2	2GT1C1	2GT1R3	3Gt4C2	3Gt3R1	4Gt1C1	4Gt1R1	5GT1PT3	5GT2PT2
Location in grain:	core	rim	core	rim	core	rim	core	rim	core	rim		
Major elements (wt%)												
SiO_2	41·76	41·32	42·08	42·34	42·40	42·76	42·16	42·50	41·69	41·03	41·27	41·24
TiO_2	0·25	0·26	0·36	0·39	0·26	0·26	0·26	0·26	0·09	0·08	0·59	0·57
Al_2O_3	16·32	16·18	19·62	19·59	20·96	21·12	21·05	20·91	17·06	16·58	15·86	15·88
Cr_2O_3	9·16	9·17	4·79	4·94	3·15	3·11	3·20	3·49	8·45	8·49	9·38	9·39
FeO	6·20	6·13	7·06	6·98	7·23	7·26	7·23	7·35	6·48	6·48	6·52	6·57
MnO	0·31	0·33	0·34	0·33	0·33	0·31	0·35	0·31	0·33	0·31	0·34	0·34
MgO	19·74	19·56	20·92	21·12	21·32	21·24	21·38	21·33	19·38	19·72	19·47	19·69
CaO	6·29	6·28	4·75	4·85	4·29	4·24	4·25	4·32	6·22	6·23	6·23	6·22
Na_2O	0·03	0·02	0·06	0·05	0·05	0·06	0·06	0·06	0·04	0·03	0·08	0·07
P_2O_5	0·02	0·03	0·03	0·02	0·03	0·03	0·03	0·03	0·02	0·02	0·04	0·03
Total	100·08	99·29	99·99	100·60	100·02	100·39	99·96	100·57	99·76	98·98	99·77	100·00
Trace elements (ppm)												
Ba	0·06	0·03	<0·152	<0·00	<0·00	0·01	<0·00	0·02	<0·00	<0·00		
Ga	4·25	3·81	7·40	7·23	6·41	6·41	5·03	5·45	5·17	5·05		
Hf	0·40	0·47	0·47	0·53	0·35	0·31	0·42	0·33	0·11	0·08		
Nb	1·74	1·89	0·36	0·33	0·39	0·38	0·41	0·39	0·66	0·66		
Ni	35·95	35·16	60·84	54·95	51·22	50·70	31·53	35·49	63·67	61·95		
Pb												
Rb	0·06	0·01	0·01	<0·00	0·01	<0·009	<0·028	0·01	<0·025	<0·037		
Sc	90·77	96·35	90·31	84·88	67·01	65·80	60·68	58·02	116·69	119·15		
Sr	0·84	0·84	0·32	0·27	0·12	0·23	0·23	0·19	0·89	0·59		
Ta												
Th	0·04	0·05	0·02	0·02	0·02	0·00	0·01	0·13	0·09	0·08		
U	0·05	0·03	0·01	0·01	0·04	0·03	0·03	0·04	0·06	0·06		
Y	3·65	3·67	9·11	9·80	14·68	13·90	16·48	15·17	2·72	2·57		
Zr	14·66	15·37	16·58	20·63	16·08	15·98	17·55	16·98	4·42	4·05		
La	0·12	0·11	0·01	0·02	0·03	0·03	0·02	0·03	0·08	0·05		
Ce	1·13	1·05	0·20	0·19	0·33	0·34	0·35	0·36	0·92	0·87		
Pr	0·29	0·28	0·06	0·07	0·09	0·09	0·09	0·11	0·25	0·26		
Nd	1·77	1·76	0·71	0·70	0·62	0·68	0·72	0·66	1·72	1·66		
Sm	0·64	0·65	0·61	0·56	0·53	0·49	0·57	0·55	0·46	0·47		
Eu	0·20	0·23	0·29	0·29	0·28	0·27	0·29	0·30	0·14	0·15		
Gd	0·64	0·68	1·01	1·12	1·22	1·22	1·40	1·33	0·43	0·40		
Tb	0·12	0·10	0·19	0·23	0·27	0·24	0·31	0·29	0·07	0·07		
Dy	2·80	2·80	1·55	1·74	2·27	2·21	2·53	2·32	0·45	0·46		
Ho	2·58	2·60	0·36	0·36	0·54	0·54	0·62	0·55	0·12	0·10		
Er	2·69	2·88	0·98	1·06	1·81	1·68	1·97	1·80	0·32	0·30		
Tm	2·79	3·16	0·15	0·16	0·28	0·26	0·32	0·29	0·07	0·04		
Yb	3·23	3·42	1·23	1·29	2·07	1·95	2·07	2·04	0·49	0·46		
Lu	4·11	3·90	0·19	0·20	0·31	0·29	0·33	0·34	0·08	0·10		

(continued)

Table 2: Continued

	Garnet									
Lithology:	Lherzolite				Dunite		Harzburgite			
Sample:	BD3697A	BD3697A	BD3697B	BD3697B	F05JM5	F05JM5	F05JM9	F05JM9	F05JM9	F05JM9
Grain:	7AGt1	7AGt1	7BGT1C2	7BGT2C1	5GT1R2	5GT2R2	9GT1C2	9GT1R2	9GT3c1	9GT3R1
Location in grain:	traverse	traverse	core	core	rim	rim	core	rim	core	rim
Major elements (wt%)										
SiO_2	41·98	41·76	41·55	41·99	40·32	40·43	41·40	41·13	41·07	41·45
TiO_2	0·26	0·25	0·19	0·19	0·45	0·46	0·08	0·09	0·10	0·09
Al_2O_3	20·94	21·21	19·46	19·61	12·21	12·36	14·69	14·50	14·59	14·66
Cr_2O_3	3·37	3·16	5·25	5·10	13·70	13·70	12·19	12·33	12·12	12·23
FeO	7·39	7·29	6·65	6·62	6·97	7·05	6·57	6·44	6·52	6·53
MnO	0·34	0·34	0·33	0·33	0·36	0·35	0·35	0·34	0·36	0·35
MgO	21·76	21·56	20·83	20·87	17·27	17·45	21·20	21·02	20·76	21·03
CaO	4·41	4·32	5·23	5·18	7·99	8·01	4·14	4·22	4·22	4·21
Na_2O	0·08	0·07	0·03	0·05	0·03	0·03	0·02	0·02	0·02	0·01
P_2O_5	0·03	0·03	0·02	0·03	0·05	0·06	0·02	0·01	0·02	0·01
Total	100·56	99·97	99·55	99·97	99·35	99·90	100·67	100·11	99·79	100·58
Trace elements (ppm)										
Ba			0·01		0·02	0·61	0·01	0·03		
Ga			6·18	6·03	7·86	7·81	3·12	3·30	3·08	
Hf			0·29	0·28	0·84	0·90	0·18	0·15	0·16	
Nb			0·49	0·44	0·99	0·99	1·13	1·10	0·91	
Ni			49·48	50·41	42·80	42·08	38·03	37·76	35·54	
Pb				0·03						
Rb			0·01	0·02	0·00	0·09	0·01	0·03	0·00	
Sc			67·62	67·64	96·71	97·91	140·30	134·84	140·95	
Sr			0·28	0·39	0·95	1·95	1·18	1·28	0·91	
Ta			0·05	0·05						
Th			0·01	0·01	0·06	0·03	0·05	0·05	0·08	
U			0·02	0·02	0·09	0·08	0·10	0·09	0·12	
Y			8·27	7·99	6·00	6·32	1·70	1·46	1·79	
Zr			10·74	10·96	38·58	38·70	5·74	5·40	6·51	
La			0·03	0·02	0·14	0·13	0·13	0·13	0·11	
Ce			0·30	0·31	1·27	1·31	1·65	1·66	1·61	
Pr			0·11	0·12	0·39	0·42	0·55	0·55	0·54	
Nd			1·21	1·18	3·34	3·28	4·13	4·05	3·84	
Sm			0·58	0·66	1·62	1·71	0·75	0·77	0·77	
Eu			0·25	0·25	0·62	0·63	0·23	0·24	0·23	
Gd			0·83	0·81	1·71	1·59	0·52	0·40	0·55	
Tb			0·15	0·15	0·22	0·21	0·07	0·06	0·06	
Dy			1·22	1·19	5·08	5·20	1·34	1·38	1·63	
Ho			0·30	0·29	4·58	4·76	1·06	1·30	1·59	
Er			0·90	0·96	4·19	4·19	1·25	1·06	1·13	
Tm			0·15	0·15	4·01	4·29	1·09	1·13	1·34	
Yb			1·21	1·16	5·16	5·16	1·24	1·61	1·80	
Lu			0·19	0·19	5·77	6·10	2·32	2·32	2·80	

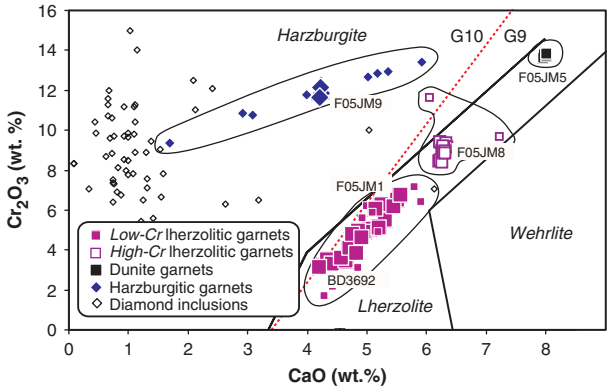

Fig. 2. Variation of CaO and Cr_2O_3 in Finsch pyrope garnets. Field boundary between G9 and G10 parageneses is indicated by a dotted line. The Finsch lherzolitic garnets exhibit an almost continuous linear variation from ~2 to 14 wt % Cr_2O_3 and plot to the low-Ca side of the lherzolite field. Field boundaries are from Dawson & Stephens (1976) and Grütter *et al.* (2006). Large symbols show data from this study (Table 2 and Supplementary Dataset). Other data (shown by small symbols) are from: Gurney & Switzer (1973); Gurney *et al.* (1979); Gurney (1984); Richardson *et al.* (1984); Shimizu & Richardson (1987); Skinner (1989); Shee *et al.* (1982); Viljoen *et al.* (1992). Specific samples discussed in the text are labelled for reference.

Garnet

Garnets in the Finsch mantle peridotites exhibit a limited range in MgO (17·3–21·9 wt %) and FeO (5·6–9·3 wt %) but show a very wide variation in CaO (1·7–8 wt %) and Cr_2O_3 (1·7–13·8 wt %) contents (Table 2; Supplementary Dataset; Gurney & Switzer, 1973; Gurney *et al.*, 1979; Shee *et al.*, 1982; Skinner, 1989; Viljoen *et al.*, 1992; Grütter *et al.*, 2006). Molar Mg/(Mg + Fe + Ca) ratios vary from 0.76 to 0.64 and indicate that the garnets are pyrope-rich. Single garnet grains have a restricted compositional range and do not show the pronounced systematic zonation that has been described from many other Kaapvaal peridotites (e.g. Smith & Boyd, 1992; Griffin *et al.*, 1999*a*; Burgess & Harte, 2004).

CaO vs Cr_2O_3 plots have been widely employed to distinguish between pyrope garnets of different parageneses and we have followed this approach (Fig. 2). On the basis of CaO and Cr_2O_3 contents and the recently updated classification scheme of Grütter *et al.* (2006), we have divided the Finsch garnets into 'lherzolitic' and 'harzburgitic' types and subsequently we refer to the host xenoliths according to these parageneses. Most of the Finsch garnets analysed in our study plot in the field of lherzolitic garnets in Fig. 2 and are G9 garnets according to the nomenclature of Dawson & Stephens (1976). This 'lherzolitic' trend indicates that the garnets were in equilibrium with clinopyroxene, although this phase was not observed in samples containing garnets with >8 wt % Cr_2O_3. We have, therefore, further subdivided the lherzolitic garnets into 'Low-Cr' (<8 wt % Cr_2O_3) and 'High-Cr' types (>8 wt % Cr_2O_3). This subdivision also correlates with the textural variations in the Finsch xenoliths; the Low-Cr lherzolitic garnets generally occur in xenoliths with coarse–tabular textures whereas the High-Cr lherzolitic garnets occur in samples that have coarse–equant grains (Table 1). The highest Cr_2O_3 (13·8 wt %) and CaO (8 wt %) contents occur in garnets in dunite F05JM5, which contains virtually no ortho- or clinopyroxene (Table 1). Zonation has been observed only in two of the Low-Cr lherzolitic garnets, where cores have lower CaO and Cr_2O_3 contents (by ~0·5 wt %) than the rims. The positive slope of the CaO vs Cr_2O_3 trend displayed by the Finsch lherzolitic garnets is defined by the equation $Cr_2O_3 = 2{\cdot}7CaO - 8{\cdot}6$ and is thought to be both temperature and pressure dependent (Griffin *et al.*, 1999*a*).

The least abundant type of garnets in the Finsch peridotites are those that plot in the field of G10 harzburgitic garnets (e.g. F05JM9, Fig. 2). These are sub-calcic garnets that contain 1·7–5·7 wt % CaO and 13·5 wt % Cr_2O_3. Their undersaturation in Ca suggests that they were not in equilibrium with clinopyroxene (Brey *et al.*, 1990). In Fig. 2, the harzburgitic garnets, and also those from dunite F05JM5, exhibit an almost continuous positive linear trend; the slope of this is slightly steeper than the isobaric trend predicted by Grütter *et al.* (2006).

The Finsch garnets display a wide variation in Al_2O_3 (12–22·5 wt %) and exhibit a negative correlation between this oxide and Cr_2O_3. Cr-number [Cr/(Cr + Al)] varies from 0·43 in the dunite, to 0·40–0·35 in the harzburgitic garnets, 0·34–0·26 in the High-Cr lherzolitic garnets, and to 0·19–0·09 in the Low-Cr lherzolitic garnets.

Peridotitic inclusions in Finsch diamonds also contain pyrope garnets. These have higher MgO contents (20–27·5 wt %; Richardson *et al.*, 1984) than garnets in the Finsch peridotites. The pyrope garnet inclusions have some of the lowest recorded CaO contents (<1·42 wt %) and have a wide range of Cr_2O_3 contents (5·4–15 wt %) and Cr-number (44–15). Molar Mg/(Mg + Fe + Ca) ratios vary from 0·93 to 0·73. On a CaO vs Cr_2O_3 plot (Fig. 2), the garnets from peridotitic suite inclusions plot in the field of harzburgitic garnets but lie away from the linear trend displayed by sub-calcic garnets in the xenolith suite.

In addition to exhibiting large differences in their major-element chemistry, the Finsch pyrope garnets have varied trace-element concentrations and ratios. The lherzolitic garnets are characterized by high Ti (500–2000 ppm), Y (2·5–16·5 ppm), Lu (0·08–0·27 ppm) and Zr contents (4–40 ppm) but low La (0·01–0·14 ppm), Sr (<0·5 ppm) and Sc (57–117 ppm) relative to the harzburgitic garnets in which Ti = 500 ppm, Y = 1·7 ppm, Lu = 0·07, Zr = 5–10 ppm, La = 0·14 ppm, Sr ~1 ppm and Sc = 135 ppm (Fig. 3). The highest contents of Sr (6–9 ppm) and lowest contents of Ti (<200 ppm) and Zr (5–8 ppm) in Finsch garnets occur in the diamond inclusions (Shimizu & Richardson, 1987). On mantle-normalized multi-element plots, all of

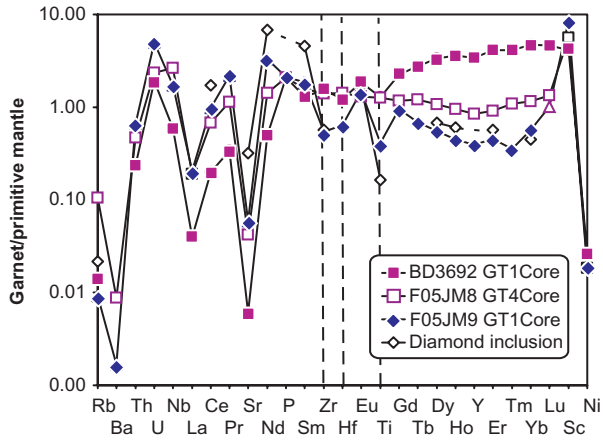

Fig. 3. Mantle-normalized concentrations of trace elements present in Finsch pyrope garnets representative of both lherzolitic (BD3692 and F05JM8) and harzburgitic parageneses (F05JM9). Elements are plotted in order of increasing compatibility during mantle melt generation. The composition of a pyrope garnet from a Finsch diamond inclusion is shown for comparison. Data sources: Table 2; Supplementary Dataset; Richardson *et al.* (1984); Shimizu & Richardson (1987). Normalization factors are from McDonough & Sun (1995).

the garnets have relative depletions at Sr and most are also depleted in Ti (Fig. 3). Additionally, the sub-calcic harzburgitic garnets have troughs at Zr and Hf.

As has previously commonly been observed in peridotite xenoliths and diamond inclusions from the Kaapvaal and other regions of cratonic lithosphere, sinuous- or 'humped'-shaped chondrite-normalized REE patterns that peak at Nd (or Sm) and have depletions at La and Er (and Tm) are typically found in the harzburgitic (sub-calcic) garnets whereas much flatter patterns with no pronounced peaks or troughs are restricted to the lherzolitic garnets (Nixon *et al.*, 1987; Shimizu & Richardson, 1987; Hoal *et al.*, 1994; Shimizu *et al.*, 1997; Stachel *et al.*, 1998). The strong LREE/HREE fractionation of the lherzolitic garnets resembles pyrope garnets that crystallize in high-temperature melting experiments in which clinopyroxene is also present (Fig. 4) (e.g. Hauri *et al.*, 1994; Salters *et al.*, 2002; Tuff & Gibson, 2007). The Finsch garnets exhibit a continuum from sinuous harzburgitic to smooth lherzolitic REE patterns with the High-Cr lherzolitic garnets displaying intermediate REE patterns (Fig. 4). The lherzolitic garnets exhibit increasing LREE and decreasing HREE with CaO content but the harzburgitic garnets plot away from these trends (Fig. 5). LREE/MREE ratios are relatively constant (e.g. $[La/Nd]_n$ ~0·5–0·15) for garnets in all lithologies. We have used chondrite-normalized Nd/Er and Er/Lu ratios as a measure of the degree of sinuosity of the REE patterns (Fig. 6). $[Nd/Er]_n$ ratios are 6–8 in the Low-Cr harzburgitic garnets, two in the dunite and High-Cr lherzolitic garnets and <1 in the Low-Cr lherzolitic garnets; we note that the highest $[Nd/Er]_n$ ratio (~12) is for a garnet from a Finsch diamond inclusion analysed by Shimizu & Richardson (1987). $[Er/Lu]_n$ ratios show the opposite variation to $[Nd/Er]_n$, being highest in the Low-Cr lherzolitic garnets (0·5–1) and lowest in the Low-Cr harzburgitic garnets (0·4). There are no Lu concentrations available for garnet inclusions in Finsch diamonds.

Olivine

In the Finsch mantle xenolith suite, olivine Mg-number ($[Mg/(Mg + Fe)] \times 100$) varies from 89·6 to 93·7 (Table 2; Supplementary Dataset; Shee *et al.*, 1982; Richardson *et al.*, 1984; Skinner, 1989; Viljoen *et al.*, 1992). The most Fe-rich olivines are present in xenoliths bearing the Low-Cr lherzolitic garnets (Mg-number = 89·6–92·1) and the dunite (91·8); Mg-rich olivines occur in samples with High-Cr lherzolitic (91·36–93·67) and harzburgitic garnets (92·6–92·94) but by far the most magnesian olivines at Finsch are those present as diamond inclusions (92·1–95·3; Table 2; Shee *et al.*, 1982; Richardson *et al.* 1984; Skinner, 1989; Viljoen *et al.*, 1992). CaO (~0·04 wt %) and NiO (0·36–0·45 wt %) exhibit little variation in Finsch olivines.

Orthopyroxene

Single orthopyroxene grains in the Finsch peridotites show no evidence of compositional zonation. They are enstatite rich and have Mg-numbers that are slightly higher than those of coexisting olivine. Orthopyroxene Mg-number varies from 91·4 in the xenoliths with Low-Cr lherzolitic garnets to 93·7 in those bearing High-Cr lherzolitic garnets. Orthopyroxene in the harzburgite (F05JM9) also has a high Mg-number (92·8) but the most magnesium-rich orthopyroxenes observed at Finsch are those present in peridotitic diamond inclusions (Mg-number = 94·4–95·5; Richardson *et al.*, 1984).

The Al_2O_3 contents of the Finsch orthopyroxenes are low (0·47–0·68 wt %) relative to those analysed from most other Kaapvaal xenolith suites (Fig. 7). They are, however, generally higher than those analysed in orthopyroxenes from Finsch diamond inclusions, which have extremely low Al_2O_3 contents (0·11–0·66 wt %; Fig. 7).

The CaO contents of Finsch orthopyroxenes vary with rock type in the same way as CaO contents in garnets; they are lowest in the sample with harzburgitic garnets (~0·4 wt %) and highest in xenoliths containing lherzolitic garnets (0·5–0·8 wt %; Fig. 7). Orthopyroxenes from harzburgitic diamond inclusions have the lowest CaO contents (<0·3 wt %) observed at Finsch. This is consistent with experimental data suggesting that CaO contents of orthopyroxene increase with temperature (Brey & Kohler, 1990) and/or increasing degree of metasomatism (see below).

TiO_2 contents of all orthopyroxenes are low (0·7–0·8 wt%). Cr_2O_3 contents of orthopyroxene are low in xenoliths bearing lherzolitic garnets (~0·3 wt %) and highest in the rare grains that occur in the dunite (F05JM5) and

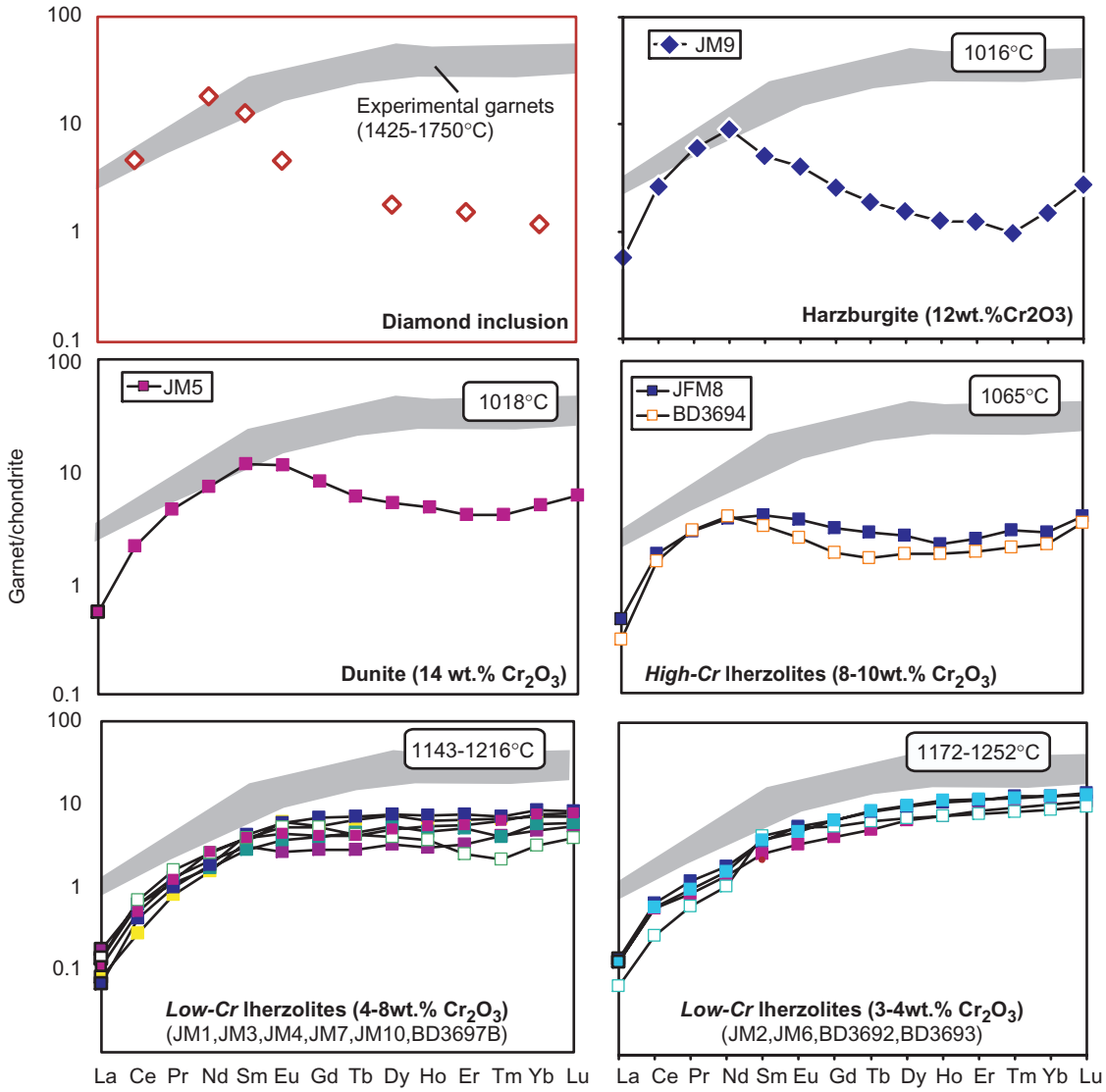

Fig. 4. Chondrite-normalized REE patterns of Finsch pyrope garnets. The field for garnet generated in 1450–1750°C experimental studies on mantle assemblages containing cpx, opx and ol is shown for comparison. Data sources: Table 2; Supplementary Dataset; Shimizu & Richardson (1987); Tuff & Gibson (2007). Temperatures were calculated iteratively using P_{BBG} (Brey *et al.*, 2008) with T_{BKN} (Brey & Kohler, 1990) and T_{ONW} (O'Neill & Wood, 1979) and are from Table 3. Chondrite-normalization factors are from McDonough & Sun (1995).

harzburgite (F05JM9; 0·5 wt %). A negative relationship exists between Cr_2O_3 and Al_2O_3 for orthopyroxene in the lherzolitic xenoliths and reflects the substitution of Al^{3+} for Cr^{3+} in the M1 cation site. A different substitution mechanism appears to occur in orthopyroxene in the dunite and harzburgite, where Cr_2O_3 contents are high for a given Al_2O_3 content. This relationship is similar to that observed in the garnets (see above) and reflects the absence of Cr-diopside in these samples such that all of the Cr partitions into garnet and orthopyroxene.

The high CaO contents of orthopyroxene in Finsch coarse–tabular garnet lherzolites, relative to those found in coarse–equant garnet lherzolites (Fig. 7), suggest that they equilibrated at higher temperatures. Furthermore, the low Al_2O_3 of orthopyroxene in the diamond inclusions and harzburgites suggests that the geothermal gradient beneath Finsch peridotites is unusually low for the Kaapvaal lithosphere and/or that they equilibrated in mantle with a low Al_2O_3 content (see below).

Clinopyroxene

At Finsch, clinopyroxene is present only in xenoliths bearing Low-Cr lherzolitic garnets and has not been observed in peridotitic diamond inclusions. As has been described for other phases, there is no evidence of compositional zonation within grains. In the Finsch peridotite xenolith suite, however, Mg-number ranges from 91·7 to 93·5 and is higher and lower, respectively, than in coexisting olivine

and orthopyroxene. Partitioning of Mg and Fe between clinopyroxene and olivine is similar to that displayed by orthopyroxene and olivine, and suggests that, for the major elements at least, these phases are in equilibrium. Ca/(Ca + Mg) in the clinopyroxene exhibits very little variation, ranging from 0·435 to 0·445. Cr_2O_3 contents vary from 1 to 2 wt %, indicating that they are Cr-diopsides (Stephens & Dawson, 1977). The Cr-diopside is rich in Na_2O (1·3–2·4 wt %) and has low to moderate contents of Al_2O_3 (1·4–3 wt %) and TiO_2 (0·04–0·17 wt %).

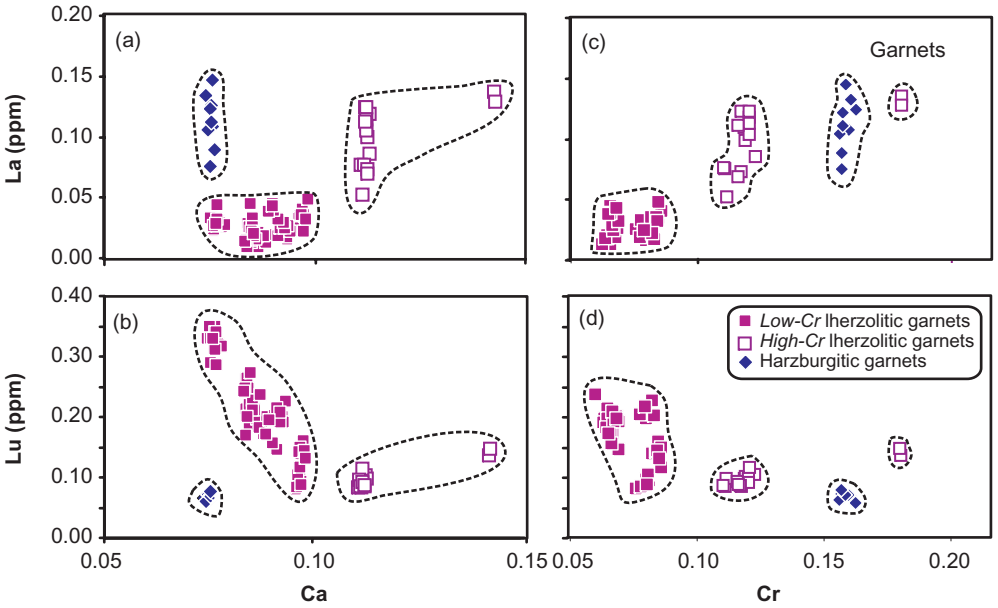

Fig. 5. Variation of molar Ca (a, b) and Cr (c, d) with an LREE, La, and an HREE, Lu, in Finsch pyrope garnets. Substitution of REE for Ca in lherzolitic garnets is believed to take place in the garnet X-cation site but analyses of harzburgitic garnets indicate a more complex substitution mechanism. Data are from Table 2 and the Supplementary Dataset.

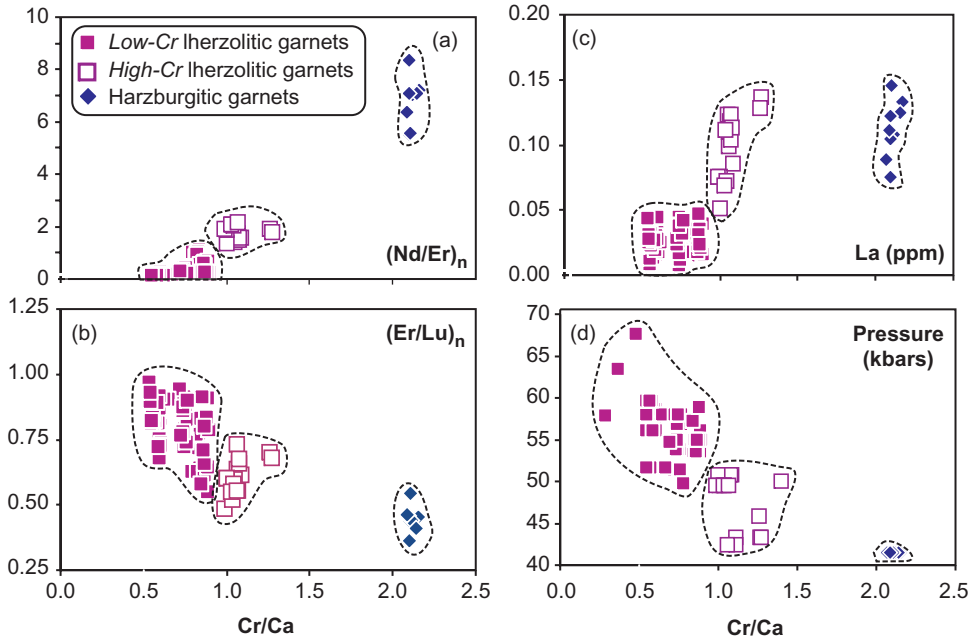

Fig. 6. Variation of garnet Cr/Ca ratio with: selected MREE and HREE ratios (a, b); and a light REE, La (c). (d) shows the pressure dependence of the Cr/Ca ratio in Finsch garnets. Data are from Tables 2 and 3, and the Supplementary Dataset. Chondrite-normalization factors are from McDonough & Sun (1995).

Cr-diopsides in xenoliths bearing very low-Cr lherzolitic garnets (BD3692, 3693, BD3697A) also have low Ca but are enriched in Cr, Al, Na and Ti relative to Cr-diopsides from samples with higher Ca lherzolitic garnets (F05JM1, 2, 3, 4, 6, 7, 10 and BD3697B; Fig. 8). Concentrations of CaO and Al_2O_3 in clinopyroxene are strongly temperature dependent but also vary with metasomatism, as do FeO, TiO_2 and Na_2O. The latter also increases with pressure (see below).

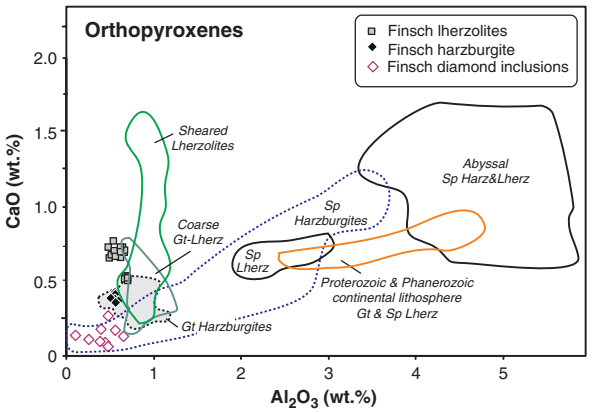

Fig. 7. Variation of Al_2O_3 and CaO in orthopyroxenes from mantle xenoliths and abyssal peridotites. (Note the very low Al_2O_3 contents of orthopyroxenes present in Finsch diamond inclusions and harzburgites.) Data sources: Table 2; Supplementary Dataset; S. A. Gibson *et al.*, unpublished data; Hervig *et al.* (1980); Cox *et al.* (1987); Boyd *et al.* (1993); Ionov *et al.* (1993); Bernstein *et al.* (1998, 2006); Brunelli *et al.* (2006); Simon *et al.* (2007).

Compatible trace elements, such as Sc, are present in similar concentrations in the Cr-diopsides but the incompatible trace elements exhibit more variation. Clinopyroxenes with the lowest Ca contents (i.e. from BD3692 and 3693) have the highest abundances of incompatible trace elements in addition to Cr, Al, Na and Ti. For example, concentrations of La range from 8·5 ppm in the 'Low-Ca' Cr-diopsides to 1·2 ppm in the 'High-Ca' Cr-diopsides. On normalized multi-element plots, the Finsch clinopyroxenes are characterized by variable (and sometimes large) negative Zr anomalies and slight but variable negative Ti and Nb anomalies (Fig. 9). These elements show variable positive anomalies on the corresponding normalized plots for coexisting lherzolitic garnets; this feature suggests that the garnet–clinopyroxene partition coefficients for Nb, Ti and Zr are greater than those for adjacent elements (K, La, Sm, Hf, Eu, Gd).

The Cr-diopsides display a large and variable fractionation of LREE and HREE with $[La/Yb]_n$ ranging from 100

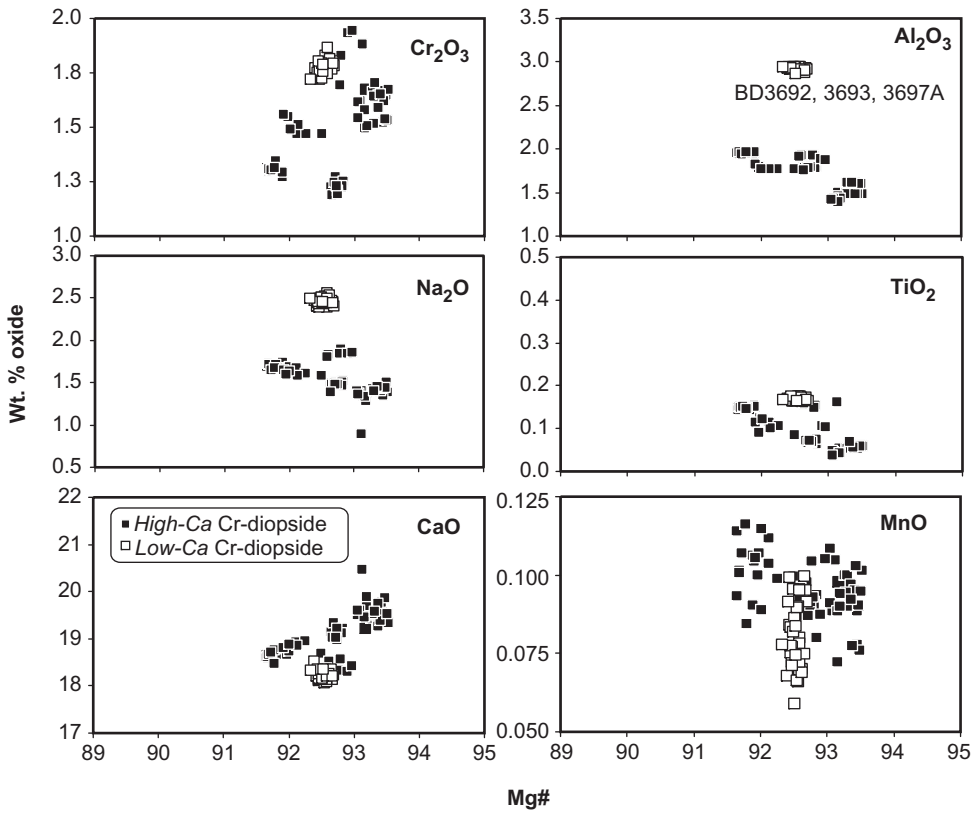

Fig. 8. Variation of Mg-number ($[Mg/(Mg + Fe)] \times 100$) with major and trace elements in Finsch Cr-diopsides. Low-Ca Cr-diopsides are present in samples BD3692, 3693 and 3267A, High-Ca Cr-diopsides occur in F05JM1, 2, 3, 4, 6, 7, 10 and BD3697B. Data are from Table 2 and the Supplementary Dataset.

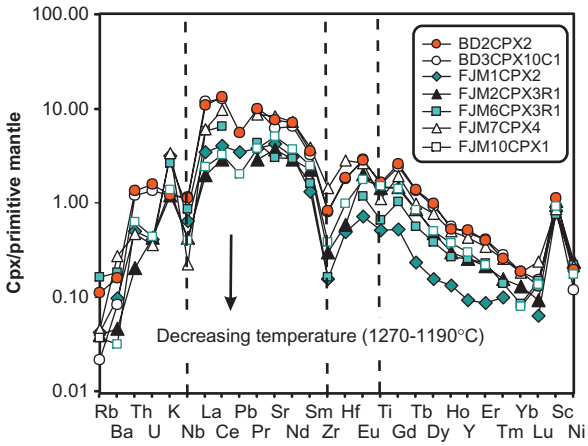

Fig. 9. Primitive-mantle-normalized multi-element patterns of Cr-diopsides from Finsch peridotites. Data are from Table 2 and the Supplementary Dataset. Normalization factors are from McDonough & Sun (1995).

to 800. Chondrite-normalized REE patterns generally peak at Ce; BD3693, 3692, 3697A and F05JM1 exhibit less fractionation of La and Ce ($[La/Ce]_n = 0{\cdot}8$–$1{\cdot}0$) than the other Cr diopsides (0·6–0·8). We have also identified subtle differences in $[Er/Lu]_n$, which, as for the garnets, are highest in the BD3693 and 3692. This suggests that, where these phases coexist, they are in chemical equilibrium. The Low-Ca Cr-diopsides (i.e. BD3692 and 3693) display peaks at Th and U relative to adjacent elements (i.e. Rb, Ba and K) on mantle-normalized multi-element plots (Fig. 9). In the High-Ca Cr-diopsides, mantle-normalized concentrations of Th and U are less than K, and $[Th/U]_n > 1$ whereas in the Low-Ca Cr-diopsides $[Th/U]_n < 1$. Our observations of Cr-diopside trace-element chemistry are consistent with the results of theoretical studies of pyroxenes (e.g. Wood & Blundy, 1997, 2001) which have shown that the REE, Ba, K, Na, Rb, Sr, Th and U reside in the large M2 cation site and that their partitioning is dependent upon the amount of replacement of Ca^{2+} by Na^{+} (i.e. $REE^{3+} + Na^{+} = 2Ca^{2+}$). Fractionation of Th and U may reflect the temperature dependence of the lattice to incorporate highly charged (4+) ions.

THERMOBAROMETRY OF FINSCH XENOLITHS

Pressure and temperature (*PT*) estimates calculated from published analyses of minerals present in Finsch xenoliths suggest that some of the samples last equilibrated at high pressures (~6 GPa) but relatively low temperatures (1250°C). These pressure estimates are some of the highest recorded for the Kaapvaal craton. Furthermore, these 'cold' and very 'deep' mantle xenoliths have been used as strong evidence that the conductive geotherm beneath the Kaapvaal craton has not been perturbed by heating events immediately prior to xenolith entrainment (Bell *et al.*, 2003).

We have employed various combinations of the most commonly used two-pyroxene solvus geothermometers (T_{BKN}, Brey & Kohler, 1990; T_{FB}, Finnerty & Boyd, 1987) together with Al-in-opx barometers (P_{BBG}, Brey *et al.*, 2008; P_{BKN}, Brey & Kohler, 1990; P_{McG}, MacGregor formulation published by Finnerty & Boyd, 1984) to estimate the pre-eruption equilibration conditions of clinopyroxene-bearing Finsch peridotites. Pressure and temperatures were calculated iteratively and the results are shown in Table 3 and Fig. 10. Pressures and temperatures for clinopyroxene-free peridotites were similarly estimated using the olivine–garnet Fe–Mg exchange thermometer of O'Neill & Wood (1979) (T_{ONW}) with P_{BBG}, P_{BKN} and P_{McG} Al-in-opx barometers. Different combinations of these geobarometers (excluding P_{BBG}) and thermometers have been used in recent studies (e.g. Bell *et al.*, 2003; Burgess & Harte, 2004; Simon *et al.*, 2007), and allow comparison of our results from Finsch with those from other Kaapvaal xenolith suites.

The recently published Al-in-opx barometer of Brey *et al.* (2008) includes results from new high-pressure (6–10 GPa) multi-anvil experiments. Pressure estimates for the Finsch lherzolites derived by combining this barometer (P_{BBG}) with T_{BKN} are up to ~13 and 16 kbar lower than those calculated using P_{BKN} vs T_{BKN} and P_{McG} vs T_{BKN}, respectively (Table 3). This equates to differences in equilibration depths of up to 50 km and has a huge effect on estimates of geothermal gradients and lithospheric thickness (see below). Despite the fact that P_{BBG} relies on the same low- to medium-pressure experimental results as P_{BKN} (2·8–6 GPa; Brey *et al.*, 1990) we note that, for Finsch lherzolites that equilibrated at shallow depths (equivalent to ~50 kbar), the pressure estimates from P_{BBG} are significantly lower than those from P_{BKN}. The P_{BBG} vs T_{BKN}/T_{ONW} combination places a diamond-bearing lherzolite (XM48; Shee *et al.*, 1982) and two diamond-bearing harzburgites (865 and 866; Viljoen *et al.*, 1992) shallower than the graphite–diamond stability field boundary (Fig. 11); only diamond-bearing xenolith XM46 (Shee *et al.*, 1982) plots in the diamond stability field. The 1σ error associated with P_{BBG} (~3 kbar; Brey *et al.*, 2008) is such that the *P* estimates for XM48 and 865 are within error of the diamond stability field. This is not the case for harzburgite 866, which plots at a significantly lower pressure than the graphite–diamond phase boundary of Kennedy & Kennedy (1976). This deviation may, however, reflect the sensitivity of T_{ONW} to Fe^{3+} (Canil *et al.*, 1994; Canil & O'Neill, 1996). The effects on *PT* estimates associated with errors in the calculation of Fe^{3+} are shown in Fig. 11. Here we have used Fe^{3+} contents calculated from Mössbauer spectroscopy to calculate equilibration pressures and

Table 3: Summary of petrographic variations and PT *estimates for Finsch mantle xenoliths*

Sample	Garnet paragenesis	Texture	P_{BBG}	T_{BKN}	P_{BBG}	$T_{O'N\&W}$	P_{BKN}	T_{BKN}	P_{BKN}	T_{FB}	P_{BKN}	$T_{O'N\&W}$	P_{McG}	T_{BKN}	P_{McG}	T_{ONW}
F05JM9	Harzburgite	Coarse-equant			34·41	1016					41·60	1048			56·53	1116
F05JM5	High-Cr Lhz	Coarse-equant			34·90	1018					44·20	1057			58·91	1118
866	Harzburgite	Coarse			35·33	1005					43·50	1040			58·41	1106
SK882	High-Cr Lhz	Coarse-equant			37·71	1018					45·80	1053			56·12	1098
BD3695	High-Cr Lhz	Coarse-equant			36·23	1051					43·10	1080			59·02	1148
SK729	High-Cr Lhz	?			39·33	1037					51·40	1087			59·48	1120
BD3694	High-Cr Lhz	Coarse-equant			39·85	1068					49·00	1107			60·52	1156
F05JM8	High-Cr Lhz	Coarse-equant			41·44	1065					51·60	1108			60·36	1146
865*	Low-Cr Lhz	Coarse			43·57	1085					52·50	1131			62·76	1177
BD3697B	Low-Cr Lhz	Coarse-tabular	45·64	1143			51·42	1152	47·97	1098			59·31	1167		
F05JM1	Low-Cr Lhz	Coarse-tabular	46·40	1176			53·51	1189	48·49	1108			63·11	1208		
XM48	Low-Cr Lhz	Coarse (tabular?)	46·65	1133			54·12	1147	52·28	1118			61·99	1162		
F05JM4	Low-Cr Lhz	Coarse-tabular	46·73	1174			53·75	1186	48·58	1106			62·54	1203		
SK695	Low-Cr Lhz	?	46·96	1181			55·69	1197	50·67	1116			63·12	1212		
BD3697A	Low-Cr Lhz	Coarse-tabular	47·92	1146			51·69	1153	47·19	1084			56·91	1163		
JJG545	Low-Cr Lhz	?	48·31	1194			56·94	1213	53·80	1175			61·63	1223		
JJG147	Low-Cr Lhz	?	48·35	1154			54·70	1171	53·33	1117			61·75	1179		
F05JM10	Low-Cr Lhz	Coarse-tabular	49·89	1206			56·81	1219	51·86	1146			63·20	1232		
F05JM7	Low-Cr Lhz	Coarse-tabular	50·30	1216			57·97	1231	51·37	1137			64·59	1245		
BD3693	Low-Cr Lhz	Coarse-tabular	50·36	1172			54·59	1180	49·15	1099			58·61	1180		
F05JM2	Low-Cr Lhz	Porphyroclastic	50·34	1207			56·11	1219	50·05	1131			62·16	1231		
JJG479	Low-Cr Lhz	?	51·96	1126			57·81	1137	55·47	1105			55·80	1133		
F05JM6	Low-Cr Lhz	Coarse-tabular	52·31	1213			58·60	1225	51·92	1128			63·99	1236		
SK880	Low-Cr Lhz	Mosaic-porphyroclastic	53·08	1229			58·86	1241	50·99	1128			63·20	1250		
SK871	Low-Cr Lhz	Granuloblastic	53·29	1166			54·72	1174	50·88	1083			57·72	1175		
XM46	Low-Cr Lhz	Coarse (Coarse-tabular?)	53·29	1213			64·63	1234	59·84	1165			69·37	1243		
BD3692	Low-Cr Lhz	Coarse-tabular	54·64	1252			59·66	1267	46·47	1068			64·74	1277		
SK691	Low-Cr Lhz	Coarse-equant	54·88	1242			67·63	1267	58·32	1157			64·75	1263		
SK725	Low-Cr Lhz	?	54·19	1187			68·08	1214	60·57	1111			63·16	1204		
SK869	Low-Cr Lhz	?	58·90	1264			63·48	1274	55·89	1168			64·99	1277		

Abbreviations of barometers and thermometers are as follows: P_{BBG}, Brey *et al.* (2008); P_{BKN}, Brey & Kohler (1990); T_{BKN}, Brey & Kohler (1990); T_{FB}, Finnerty & Boyd (1987); T_{ONW}, O'Neill & Wood (1979); P_{McG}, Finnerty & Boyd (1984). Pressures are given in kbar and temperatures in°C. Data sources are Table 3; Gurney *et al.* (1979); Shee *et al.* (1982); Skinner (1989); Viljoen *et al.* (1992).
*No cpx analysis available for this sample.

temperatures for the one Finsch sample (865) for which there are published data (Canil & O'Neill, 1996). This diagram shows that increasing the Fe^{3+} content of both garnet and orthopyroxene to those accurately determined for this harzburgite will increase estimates of both temperature and pressure derived from P_{BBG} vs T_{ONW}. Nevertheless, T_{BKN} is insensitive to calculation of Fe^{3+} and problems associated with the estimation of this from microprobe analyses cannot explain why a diamond-bearing lherzolite from Lesotho (BD2125; Dawson & Smith, 1975) plots in the graphite stability field (Fig. 11).

Using the previously widely used P_{BKN} vs T_{BKN} combination, four literature samples (XM46, SK869, 691, 725) gave very-high pressure estimates (63–68 kbar). These xenoliths contain orthopyroxenes with a low jadeite component (because of low Na and/or high Ti; Shee *et al.*, 1982; Skinner, 1989), which causes an overestimate of pressure by ~6 kbar and the xenoliths plot well below the

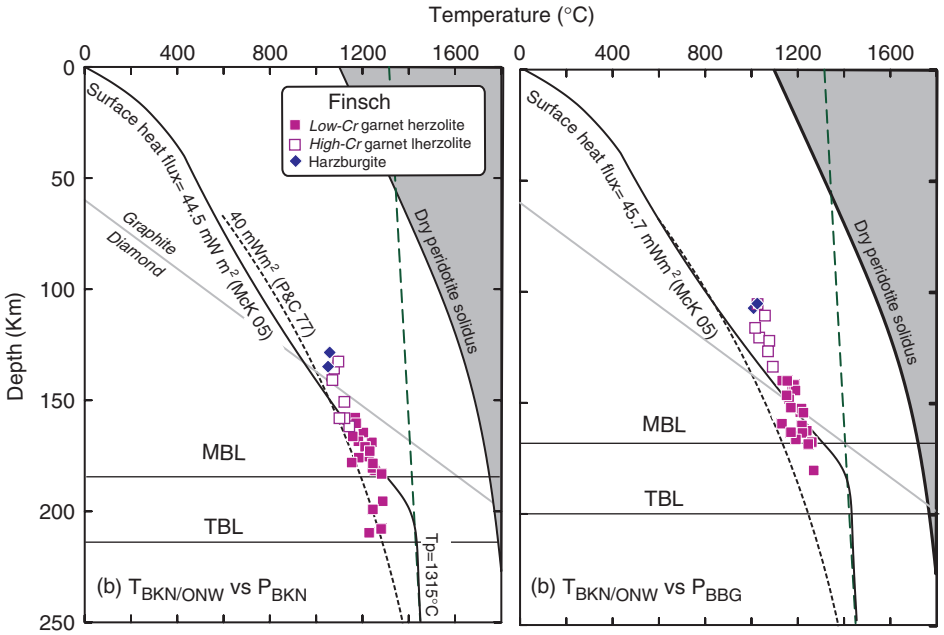

Fig. 10. Pressure vs temperature plots for Finsch mantle xenoliths. These were calculated using the two-pyroxene solvus geothermometer of Brey & Kohler (1990; BKN), the olivine–garnet Fe–Mg exchange thermometer of O'Neill & Wood (1979; ONW) and Al-in-opx barometers of Brey & Kohler (1990; BKN) and Brey *et al.* (2008; BBG). The geothermal gradient in the mechanical and thermal boundary layers (MBL and TBL, respectively) was calculated using the program FITPLOT of McKenzie *et al.* (2005), which uses variable conductivity values. The calculated surface heat flux is shown adjacent to each geotherm. Shown for reference are: the constant conductivity 40 mW m^2 surface heat-flux geotherm of Pollack & Chapman (1977), the graphite–diamond phase boundary (Kennedy & Kennedy, 1976), and the dry peridotite solidus and the adiabat for ambient Phanerozoic mantle with a T_p of 1315°C.

geotherm (see below). Using the P_{BBG} vs T_{BKN} combination, we note that lherzolites SK725, SK871 and SK869 (together with JJG470; Gurney *et al.*, 1979) have much shallower pressure estimates but plot well below the geotherm defined by other Finsch samples (Fig. 10a); this may indicate analytical problems or the presence of disequilibrium phases.

Temperature and pressure estimates for Finsch peridotites with Low-Cr lherzolitic garnets are in the range of 1130–1265°C (T_{BKN}) and 45–59 kbar (P_{BBG}), respectively (Table 3), and the xenoliths show a systematic change in temperature with depth (Fig. 10*b*). According to *PT* estimates determined using P_{BBG} vs T_{ONW}, the cpx-free peridotites (which include xenoliths with High-Cr lherzolitc garnets) equilibrated at the lowest temperatures (1000–1070°C) and pressures (34–42 kbar) and all plot above the diamond–graphite phase boundary (Fig. 10*b*). As beneath other parts of the Kaapvaal craton (e.g. Jagersfontein and northern Lesotho), *PT* estimates suggest that the harzburgites are derived from the shallowest depths (Burgess & Harte, 1999; Simon *et al.*, 2003; S. A. Gibson *et al.*, unpublished data). We note that several of the cpx-free peridotites plot above the geotherm (Fig. 10*b*). This may be due to the sensitivity of the olivine–garnet Fe–Mg exchange thermometer of O'Neill & Wood (1979) to the calculation of Fe^{3+} as described above.

We have used the results of our *PT* calculations for the Finsch xenoliths to estimate the thickness of the mechanical and thermal boundary layers beneath the west of the Kaapvaal craton. This part of the craton was unaffected by the 2 Ga Bushveld magmatic event. Seismic studies have produced varied thickness estimates for the lithosphere beneath Finsch, ranging from ~250 to 300 km (James & Fouch, 2002) and 180 km (Li & Burke, 2006; Priestley & McKenzie, 2006). If we assume a crustal thickness of 38 km (Nair *et al.*, 2006) and a mantle potential temperature of 1315°C, the Finsch samples fall on a geotherm with a surface heat flux of 44·5 mW m^2 (P_{BKN} vs T_{ONW}/T_{BKN}; Fig. 10*a*) or 45·7 mW m^2 (P_{BBG} vs T_{ONW}/T_{BKN}; Fig. 10*b*). These palaeogeotherms intersect the diamond–graphite phase boundary at depths of 135 and 150 km, respectively. This geothermal gradient is slightly hotter than has sometimes been calculated in previous studies (35–40 mW m^2, e.g. Finnerty & Boyd, 1987; Griffin *et al.*, 2003) and reflects the fact that we have used the constant lithospheric mantle heat-flux values of McKenzie *et al.* (2005) to calculate the conductive geotherm rather than the commonly used variable conductivity values of Pollack & Chapman (1977). Assuming that the temperature of the convecting mantle was 1315°C immediately prior to eruption of the Finsch kimberlite, our calculations show that the base of the Cretaceous mechanical boundary

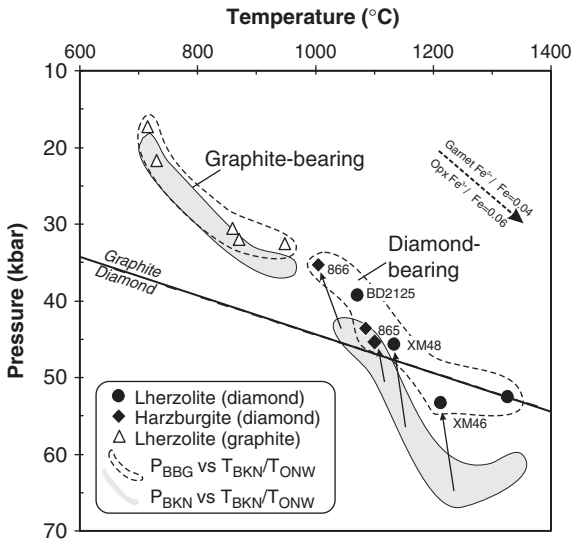

Fig. 11. Temperature vs pressure plot to show the variation in estimates for Finsch diamond-bearing peridotites using results calculated iteratively using the Al-in-opx barometers of Brey & Kohler (1990; P_{BKN}) and Brey *et al.* (2008; P_{BBG}) with the two-pyroxene solvus thermometer of Brey & Kohler (1990; T_{BKN}) and the olivine–garnet Fe–Mg exchange thermometer of O'Neill & Wood (1979; T_{ONW}). Symbols denote the *PT* estimates obtained using the Brey *et al.* (2008) barometer and various thermometers. Sample numbers of Finsch diamond-bearing harzburgites and lherzolites are shown for reference. Data are from Shee *et al.* (1982) and Viljoen *et al.* (1992). Continuous-line arrows indicate the change in *PT* estimates for single Finsch samples using the different formulations. Dashed arrow shows the magnitude of the change in temperature and pressure that result if garnet $Fe^{3+}/Fe = 0{\cdot}04$ and orthopyroxene $Fe^{3+}/Fe = 0{\cdot}06$. These values were estimated for garnet and orthopyroxene in Finsch xenolith 865 from Mössbauer spectroscopy data by Canil & O'Neill (1996). *PT* estimates for other diamond- and graphite-bearing peridotites (Dawson & Smith, 1975; Sobolev *et al.*, 1984; Pearson *et al.*, 1994) are also shown. The graphite–diamond phase boundary is from Kennedy & Kennedy (1976).

layer (MBL) would have been at a depth of 181 km or 165 km for conductive mantle geotherms of 44·5 mW m^2 (P_{BKN} vs T_{ONW}/T_{BKN}) or 45·7 mW m^2 (P_{BBG} vs T_{ONW}/T_{BKN}), respectively. If, however, we assume that the T_p of the sub-Kaapvaal convecting mantle was 1500°C at the time of Finsch kimberlite genesis (i.e. the region was underlain by a mantle plume), then the base of the Cretaceous Kaapvaal MBL may have been at a depth of ~208 km (P_{BKN} vs T_{ONW}/T_{BKN}) or 190 km (P_{BBG} vs T_{ONW}/T_{BKN}). These estimates of Cretaceous lithospheric thickness, regardless of the different combinations of geobarometers and thermometers used in the xenolith *PT* estimates, are similar to those of 180 ± 20 km suggested for the present-day Kaapvaal keel by Li & Burke (2006) and Priestley & McKenzie (2006).

MINERAL–MELT PARTITION COEFFICIENTS

Mineral–melt partition coefficients (*D* values) for trace elements are strongly linked to the major-element composition of an individual phase, which is controlled by the prevailing *PT* conditions and the bulk-rock composition. *D* values are usually determined from the results of experimental studies but most of these are undertaken at much higher temperatures than those existing in the lithospheric mantle. Partition coefficients derived from natural lithospheric mantle assemblages of equilibrium phases are therefore believed to be more appropriate for mantle xenolith studies (Harte *et al.*, 1996). Burgess & Harte (2004) calculated $D^{Grt-melt}$ values over a range of temperatures (900–1400°C) by combining ion-probe analyses of coexisting garnets and clinopyroxenes with the experimentally determined low-alumina $D^{Cpx-melt}$ values of Grutzeck *et al.* (1974) and Hart & Dunn (1993). Their calculations used $D^{Cpx-melt}$ values determined at 1380°C (Hart & Dunn, 1993) and 1265°C (Grutzeck *et al.*, 1974) and ignored any dependence of *D* values on temperature. A recent study by Tuff & Gibson (2007) has, however, shown that $D^{Cpx-melt}$ values decrease by ~20% with a 100°C increase in temperature.

We analysed adjacent grains of Cr-diopside and garnet in four Finsch peridotites that last equilibrated between 1150 and 1230°C for 26 trace elements by LA-ICP-MS. To calculate $D^{Grt-melt}$ values for all of the 14 REE, Y and Sc we estimated, using the lattice-strain model of Blundy & Wood (1994, 2003) and Wood & Blundy (1997), and the data of Hart & Dunn (1993), the theoretical $D^{Cpx-melt}$ values at 1200°C. The lattice-strain model of Blundy & Wood (1994) is able to predict REE partitioning behaviour, which is commonly expressed by plotting the partition coefficient as a parabolic function of the ionic radius of a given REE (Fig. 12). The parabola varies in height and width with varying pressure, temperature and composition. Hart & Dunn (1993) published analyses for only eight REE in their original experimental dataset and so we extrapolated the results of our lattice strain model to estimate *D* values for the remaining REE (Fig. 12 and Table 4). We used the published $D^{Cpx-melt}$ values of Hart & Dunn (1993) for the remaining trace elements and then followed the method of Harte *et al.* (1996) and Burgess & Harte (2004) to estimate $D^{Grt-melt}$ values (Table 4). For the REE, our results are similar to those determined for natural (Burgess & Harte, 2004) and synthetic pyrope garnets (Van Westrenen *et al.*, 2000) (Fig. 13). We note that our $D^{Grt-melt}$ values for Lu, which range from 6·5 to 10·2, are ~50% lower than those estimated by Burgess & Harte (2004) but are consistent with those predicted by lattice-strain models (Fig. 12).

When plotted against ionic radii, the $D^{Grt-melt}$ values that we have obtained for the REE, Sc and Y from the Finsch xenoliths display a parabolic pattern (Fig. 12) and conform closely to the partition coefficients predicted by the lattice-strain model of Blundy & Wood (1994, 2003). The parabolic pattern of $D^{Grt-melt}$ values displayed in

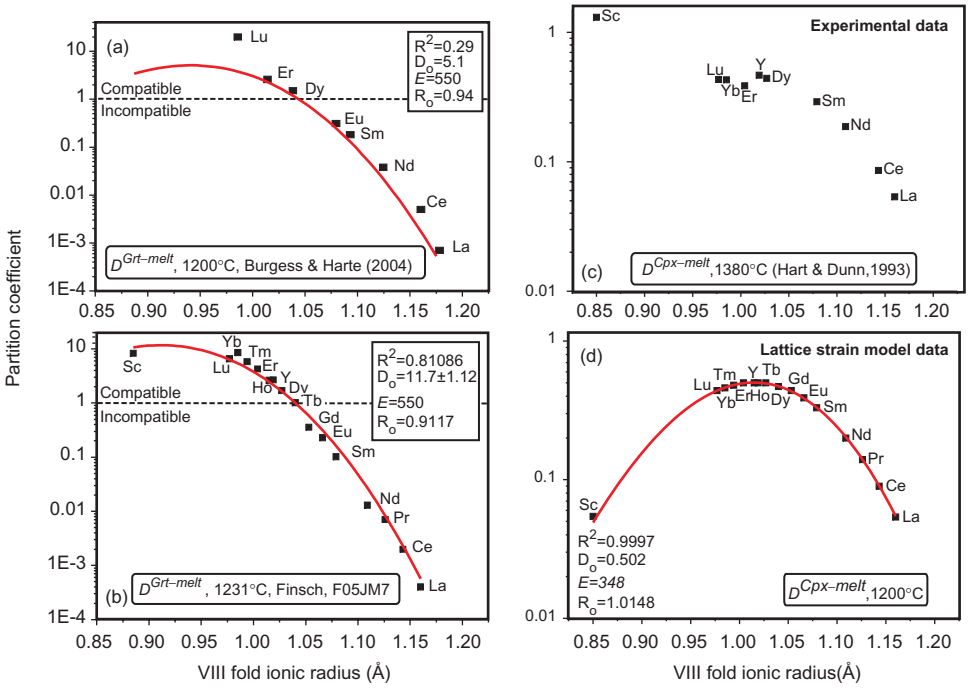

Fig. 12. Onuma diagrams showing the variation of mineral–melt partition coefficients for garnets (a, b) and clinopyroxene (c, d). Garnet–melt partition coefficients were calculated from analyses of adjacent grains of clinopyroxene and garnet using the method described in the legend for Table 4. (c) shows the $D^{\mathrm{Cpx-melt}}$ values determined from the experimental study of Hart & Dunn (1993) which was conducted at 1380°C. (d) shows the $D^{\mathrm{Cpx-melt}}$ values calculated from the non-linear least-squares fit to these experimental data at 1200°C using the lattice strain model of Blundy & Wood (1994). Continuous curves represent non-weighted Levenberg–Marquardt type, non-linear least-squares fits to equation (1) of Blundy & Wood (1994).

Fig. 12 confirms that all of the REE were in equilibrium in the adjacent grains of garnet and clinopyroxene. In xenolith suites that exhibit REE disequilibria between these phases (as has been shown for northern Lesotho; e.g. Simon *et al.* 2003) the calculated $D^{\mathrm{Grt-melt}}$ values display a sigmoidal trend when plotted against ionic radii (S. A. Gibson *et al.*, unpublished data). We have used the equations of Blundy & Wood (1994) to calculate the strain-free partition coefficient (D_{i}) for an X-cation site with an effective radius of 0·0912 nm and a Young's modulus of 550 GPa. The (D_{i}) value (11·7) that we have obtained for the parabolic dependence of the REE and Sc in the octahedral site in Finsch garnets is higher than that predicted for pyrope garnets in experimental studies (4·8) but reflects the lower equilibration temperatures of the former (1150–1250°C) relative to the latter (1425–1550°C; Van Westrenen *et al.*, 1999; Tuff & Gibson, 2007).

CAUSE OF SINUSOIDAL REE PATTERNS IN SUB-CALCIC GARNETS

The high LREE concentrations in sub-calcic harzburgitic garnets, relative to those of lherzolitic garnets, are inconsistent with their formation as single-stage melting residues of a fertile lherzolite source. Various hypotheses have been proposed to account for this discrepancy and also the difference in shape of the REE patterns exhibited by lherzolitic and harzburgitic garnets.

(1) *Slow rates of diffusion of HREE.* Hoal *et al.* (1994) and Shimizu *et al.* (1997) suggested that only the lherzolitic garnets had reached full equilibrium with an infiltrating metasomatic melt. They interpreted variations in REE patterns as a result of chemical modification or fractionation of garnet, and suggested that sinusoidal patterns reflected decreasing rates of REE diffusion with decreasing ionic radius. Such a 'disequilibrium metasomatism' hypothesis is not, however, supported by more recent work, which has shown that REE with different ionic radii have similar diffusion coefficients (Van Orman *et al.*, 2002).

(2) *Limited equilibrium with a metasomatic carbonatite melt.* Griffin *et al.* (1999*b*) proposed that sinuous REE patterns are due to the reduced number of cation sites available for LREE substitution in low-Ca (harzburgitic) garnets relative to those in high-Ca (lherzolitic) garnets. In the Finsch peridotites only the lherzolitic garnets show a good correlation between Ca and LREE concentration (Fig. 5) and incorporation of LREE into the sub-calcic garnets appears to involve a different substitution mechanism.

Table 4: Garnet–melt partition coefficients

	Xenoliths					Experimental
	Finsch				Kaapvaal (Burgess	FCMAS (Van
Sample:	BD3693	F05JM7	BD3679A	F05JM10	& Harte, 2004)	Westrenen *et al.*, 2000)
Composition:	$Py_{75}Gr_{11}Alm_{14}$	$Py_{73}Gr_{12}Alm_{15}$	$Py_{75}Gr_{11}Alm_{14}$	$Py_{74}Gr_{12}Alm_{14}$		$Py_{72}Gr_{19}Alm_{9}$
Pressure:	5·49	5·78	5·17	5·68		3
Temperature:	1227	1231	1153	1219	1200	1540
Th	0·003	0·023	—	0·012	—	0·026
U	0·014	—	0·009	0·024	—	0·038
K	0·001	—	—	—	—	—
Pb	0·005	—	0·008	0·012	—	—
Nb	0·003	0·045	0·004	0·01	—	0·017
Ta	0·008	—	0·006	0·023	—	0·024
Zr	0·2	0·11	0·27	0·75	—	0·39
Hf	0·12	0·1	0·16	0·33	—	0·38
Sr	0·0007	0·0002	0·0002	0·0007	—	0·02
La	0·0004	0·0004	0·0003	0·0006	0·0007	0·018
Ce	0·002	0·002	0·001	0·002	0·005	—
Pr	0·005	0·007	0·006	0·005	—	0·043
Nd	0·014	0·013	0·019	0·016	0·038	—
Sm	0·109	0·102	0·128	0·099	0·181	0·23
Eu	0·226	0·235	0·273	0·228	0·311	—
Gd	0·384	0·365	0·423	0·448	—	—
Tb	0·87	1·02	1·09	1·05	—	1·16
Dy	1·49	1·71	2·11	1·73	1·495	—
Y	3·24	2·83	3·39	4·31	—	—
Ho	3·58	2·64	3·66	2·88	—	—
Er	4	4·27	5·48	4·54	—	2·4
Tm	6·78	5·81	8·38	5·92	2·59	—
Yb	9·59	8·55	9·56	8·24	—	5·14
Lu	8·13	6·59	10·2	6·55	19·81	6·29
Sc	4·18	8·34	4·58	6·83	—	4·41
Ti	0·72	1·08	0·65	1·24	—	0·2

Pressures are given in kbar and temperatures in°C. Adjacent grains of clinopyroxene and garnet were analysed by LA-ICP-MS (see analytical techniques). Garnet-melt partition coefficients were then calculated using the equation $D_{\mathrm{Y}}^{\mathrm{Grt-melt}} = D_{\mathrm{Y}}^{\mathrm{Cpx-melt}} \div \chi_{\mathrm{Y}}^{\mathrm{Cpx}}/\chi_{\mathrm{Y}}^{\mathrm{Grt}}$, where D is the mineral–melt partition coefficient of element Y and χ is the concentration of element Y in a given phase. $D^{\mathrm{Cpx-melt}}$ values are from the experiments of Hart & Dunn (1993) conducted at 1380°C and 3 GPa. We used the equations of Blundy & Wood (2003) to recalculate the $D^{\mathrm{Cpx-melt}}$ values of Hart & Dunn (1993), for the REE and Y, to a temperature similar to that at which the Finsch xenoliths last equilibrated (1200°C). Otherwise, the method for calculating garnet–melt partition coefficients is exactly the same as that of Harte *et al*. (1996) and Burgess & Harte (1999). Estimates of garnet–melt partition coefficients derived from recent studies on peridotite xenoliths and synthetic experiments are shown for comparison.

(3) *Garnet fractionation from ascending metasomatic silicate melts*. Burgess & Harte (2004) suggested that the compositions of ascending metasomatic melts control the REE patterns of mantle garnets. They proposed that high-pressure garnet fractionation caused depletion of HREE in the metasomatic melt, which subsequently ascended through the lithospheric mantle and crystallized sub-calcic garnets with 'humped' REE patterns.

(4) *Spatial and temporal variations in melt/rock ratios*. Wang *et al*. (2000) proposed that the behaviour (open or closed

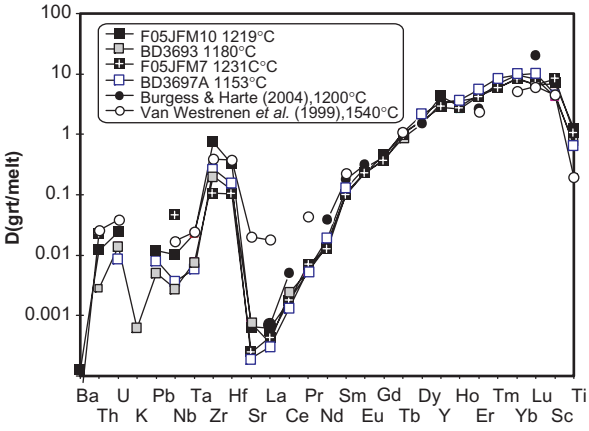

Fig. 13. Garnet–melt partition coefficients calculated from coexisting adjacent garnet–clinopyroxene grains in Finsch lherzolites. Published $D^{\mathrm{Grt-melt}}$ values of Van Westrenen *et al.* (1999) and Burgess & Harte (2004) and are shown for comparison. Data are from Tables 3 and 4.

system) of infiltrating metasomatic melts would depend on the distribution and proportion of veins relative to the host rock. Chemical equilibrium of garnet and an infiltrating LREE-rich carbonatite melt will be achieved only by the open-system behaviour that occurs when there is a high melt/rock ratio. Wang *et al.* (2000) proposed that sub-calcic garnets form in systems where the melt/rock ratio is low and that do not achieve this equilibrium.

(5) *Multi-stage tectonomagmatic processes.* It has been suggested that the sinuous REE patterns displayed by harzburgitic garnets reflect their multi-stage formation. Stachel *et al.* (1998) proposed a tectonomagmatic model involving the following sequence of events: (a) polybaric melting, initially in the garnet stability field and extending into the spinel stability field, resulting in harzburgite formation and removal of the LREE and MREE from the residue; (b) lithospheric thickening to levels at which garnet is the stable aluminous phase, causing HREE fractionation; (c) metasomatism of harzburgite by percolating methane-rich fluids with variable Si and high LREE/HREE ratios, which were also involved in diamond formation. Similar models have been invoked by Bell *et al.* (2005), Westerlund *et al.* (2006) and Simon *et al.* (2007), who proposed that the subduction-related fluids were Si-rich and associated with the transformation of olivine to orthopyroxene.

Relationship between major elements (Ca and Cr) and REE partitioning in mantle garnets

Few data are available on the substitution mechanisms of trivalent cations, such as the REE, in natural garnets. In synthetic systems (e.g. CMAS and FCMAS), the REE are thought to substitute for Ca in the garnet X-cation site. Experimental studies of pyrope garnets have shown that a large change in grossular content ($Py_{82}Gr_{18}$ to $Py_{15}Gr_{85}$) has a greater effect on D values for the LREE than for the HREE. This is because the solid solution between pyrope and grossular garnet is non-ideal and causes non-linear elasticity, which has a more significant influence on the partitioning of larger ions; that is, the LREE (Ballaran *et al.*, 1999). However, over the range of grossular contents present in pyrope garnets from mantle peridotites ($Py_{70-80}Al_{17-20}Gr_{8-14}$) fractionation of $D^{\mathrm{Grt-melt}}_{\mathrm{LREE/HREE}}$ values is small. In the Finsch lherzolitic garnets there is a reasonable correlation between Ca and LREE and HREE contents (Fig. 5) confirming that REE substitution is dependent on the amount of Ca in the X-cation site of these garnets. Such a relationship does not exist, however, when sub-calcic (harzburgitic) garnets are included in the dataset. This suggests that it is not simply the Ca content and hence pyrope:grossular ratio that controls the REE patterns of peridotitic garnets.

When garnets present in both lherzolitic and harzburgitic parageneses at Finsch are considered, the LREE show a much better correlation with Cr/Ca than Ca content (Figs 5 and 6). The relationship between Cr^{3+} and REE fractionation does not appear to be a charge-balancing effect of the trivalent REE in the garnet X-cation site, by substitution of Al^{3+} in the Z site, because there is no Si^{4+} deficiency and $Al^{3+}+ Cr^{3+} \leq 2$ cations per formula unit. Significant substitution of Al by the larger Cr cation will, however, increase the effective radius of the garnet octahedral Y site and cause a large amount of distortion of the garnet framework. This will result in enlargement of the X-cation site (Van Westrenen *et al.*, 2000). Such behaviour appears to be exemplified by the Finsch garnets, where there is greater preferential substitution of large cations (i.e. Sr and the LREE) in the high-Cr garnets. It may also explain the apparent restriction of high Sr contents (>30 ppm) to G10 garnets (Pearson *et al.*, 2003).

Our findings agree with the results of the experimental study of Wang *et al.* (1998), who examined the influence of Cr on garnet–melt REE partitioning by undertaking high-temperature (1900–2100°C) and high-pressure (7·5 GPa) experiments on garnets doped with variable amounts of Cr_2O_3 (0–14 wt %). The results of their study suggest that $D^{\mathrm{Grt-melt}}_{\mathrm{LREE}}$ values increase with, and are more affected by, Cr content than $D^{\mathrm{Grt-melt}}_{\mathrm{HREE}}$ values. Furthermore, the large amount of substitution of Al^{3+} by Cr^{3+} in the sub-calcic garnets present in the Finsch xenoliths and diamond inclusions would limit the replacement of Al in the garnet Y-cation site by Ti, Zr and Hf. This is consistent with the observations that we have outlined above and would account for the relative depletions of these trace elements on a normalized multi-element plot (Fig. 3).

P–T–X dependence

Experiments producing lherzolite assemblages have been conducted at temperatures between 1425 and 1750°C

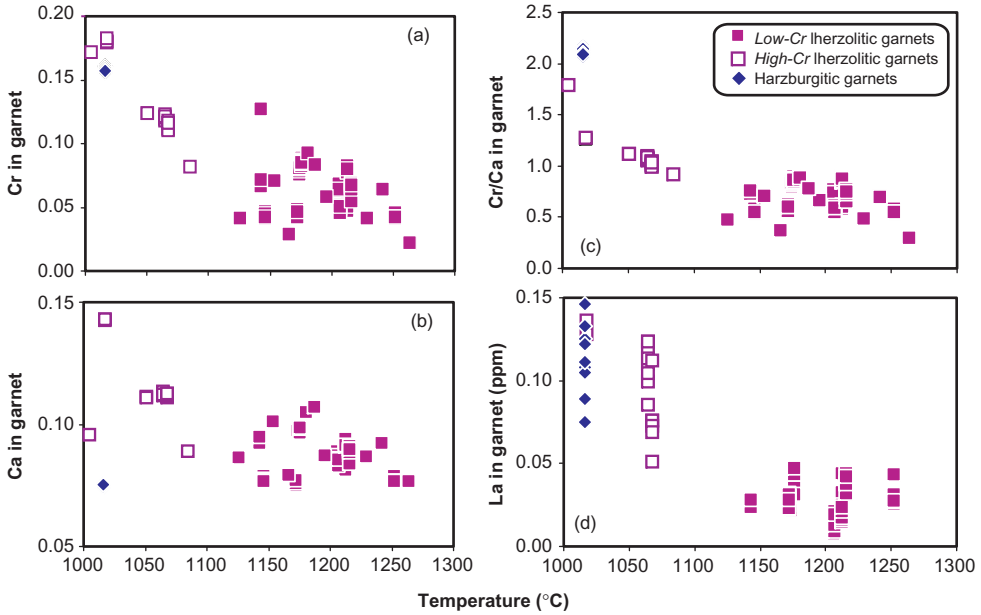

Fig. 14. Variation of xenolith equilibration temperature, calculated iteratively using the parameterizations of O'Neill & Wood (1979), Brey & Kohler (1990) and Brey *et al.* (2008), with major and trace elements in Finsch garnets. The anomalous behaviour of Ca with temperature in the harzburgite (F05JM9) should be noted. Data sources: Tables 2 and 3; Gurney & Switzer (1973); Gurney *et al.* (1979); Shimizu & Richardson (1987); Skinner (1989); Viljoen *et al.* (1992).

(e.g. Salters *et al.*, 2002; Tuff & Gibson, 2007) and have generated pyrope garnets with variable CaO (3–6 wt %), low Cr_2O_3 (<1·7 wt %) and high Al_2O_3 contents (~22 wt %). These studies have shown that partitioning of the REE into garnet is dependent on temperature as well as Ca content. This is because contraction of the garnet lattice during cooling causes an increase in elasticity, which allows enhanced substitution of large cations into the garnet X site. Hence the amount of Ca substitution by the LREE in pyrope garnets crystallizing in equilibrium with clinopyroxene decreases with increasing temperature. We have shown above, however, that Ca shows a good correlation with temperature only if the harzburgitic garnet data are excluded, so, although this might explain variations in LREE in the lherzolitic garnets, a different mechanism is necessary to explain the high partitioning of LREE into sub-calcic high-Cr garnets, such as those present in F05JM9.

The Finsch garnets display a good correlation between Cr, the LREE and also Cr/Ca ratio with temperature (Fig. 14). The dependence of LREE concentrations on Cr/Ca ratio is not readily apparent in lherzolitic garnets because Cr contents are generally low. As a consequence, lherzolitic garnets show reasonable correlations between Ca and LREE, but in harzburgitic garnets, where Cr contents are high and Ca contents low, this relationship breaks down. Substitution of Cr^{3+} for Al^{3+} in the garnet Y-cation site is known to decrease with pressure and slightly with temperature (Nickel, 1989; Ryan *et al.*, 1996; Grütter *et al.*, 2006). As temperature and pressure increase, the radius of the garnet X-cation site will decrease and inhibit substitution of large for small ions (such as Cr^{3+} for Al^{3+}); Sr and the LREE will also fit less readily into the garnet structure than the HREE. This may explain, to some extent, the relatively low LREE concentrations in the high-pressure and -temperature Finsch lherzolitic garnets (Figs 6*c,d* and 14*d*).

Another important factor that may have influenced trace-element concentrations and ratios in the Finsch garnets may be bulk-rock composition. The subcalcic garnets occur in harzburgites, which are present at shallower depths than the lherzolites. It might be argued that the lack of clinopyroxene results in the LREE and Cr partitioning more readily into the harzburgitic garnets. Griffin *et al.* (1999*c*) showed that there is a negative relationship between garnet Cr_2O_3 content and bulk-rock Al_2O_3. Bulk-rock Al_2O_3 will be influenced by the degree of partial melting involved in the initial formation of the lithospheric mantle, but it will also be affected by the degree of subsequent metasomatism (see below). The amount of metasomatism is dependent upon pressure and temperature as well as the volume and composition of the infiltrating melt or fluid. Small volumes of metasomatic melts or fluids will readily lose heat to their surroundings such that their ascent may be limited and enrichment will be concentrated at the base of the lithosphere. At Finsch, where we see a continuous variation in both REE patterns and also equilibration pressures and temperatures, we believe that both crystal chemistry and bulk-rock composition are

important in determining the partitioning of LREE into garnets. Elsewhere, the situation may be much more complex, and it may be fortuitous that at Finsch, where there have not been multi-phase metasomatic events, we have been able to see this relationship. Further studies of unzoned garnets from xenoliths with well-constrained *PT* estimates are required to establish the significance of one or both of these processes in LREE partitioning.

Garnet crystallization and HREE fractionation

Sinusoidal chondrite-normalized REE patterns with positive HREE slopes characterize pyrope garnets that occur in clinopyroxene-free Finsch peridotites and all occur in xenoliths that last equilibrated at temperatures <1100°C (Fig. 4). As we shall show below, the harzburgites appear to represent the residue of large-degree polybaric melt extraction predominantly in the spinel stability field (1·5 GPa). Because of the absence of residual garnet, at such low pressures and large degrees of partial melting, we believe that it is unlikely that the positive $HREE_n$ slope is linked to the mantle melting event that caused the initial formation of the harzburgite (see Stachel *et al.*, 1998). Instead, we examine the role of metasomatic agents that may have infiltrated the harzburgites after their formation and caused the HREE fractionation.

Figure 12 shows that the partitioning of Yb, Tm and Lu relative to Er is very different for garnet and clinopyroxene. In clinopyroxenes these elements, and also the LREE and MREE, have lower *D* values than Er, whereas garnets exhibit a negative correlation between ionic radius and *D* value for all of the REE. This is because the effective radius (r_o) of the cation site into which the REE partition in clinopyroxene is ~0·1 nm (i.e. Er) whereas in pyrope garnets r_o is ~0·09 nm (i.e. Lu). Additionally, Harte *et al.* (1996) have shown from studies of mantle xenoliths that $D^{Cpx/Grt}$ ratios for most of the REE are strongly temperature dependent; $D^{Cpx/Grt}$ values for large ions such as Nd exhibit a negative correlation with temperature whereas elements with a smaller ionic radius (such as Lu) have a positive correlation. $D^{Cpx/Grt}$ for Er, however, exhibits very little variation so that $[Nd/Er]_n$ and $[Er/Lu]_n$ ratios for garnets in equilibrium with clinopyroxene show opposite trends when plotted against temperature (Fig. 15). At first sight this may explain why pyrope garnets from Finsch xenoliths exhibit differences in their HREE ratios. It might be assumed that when clinopyroxene ceased to crystallize (i.e. in the lower temperature Finsch peridotite) there would be more Tm, Yb and Lu relative to Er in the melt available for partitioning into garnet; this would produce sinusoidal chondrite-normalized REE patterns with $[Nd/Er]_n \geq 1$ and $[Er/Lu]_n \leq 1$. However, because the HREE are incompatible in clinopyroxene (i.e. $D^{Cpx-melt}$ values are <1, Fig. 12), the lack of clinopyroxene crystallization from the melt has little effect on HREE ratios.

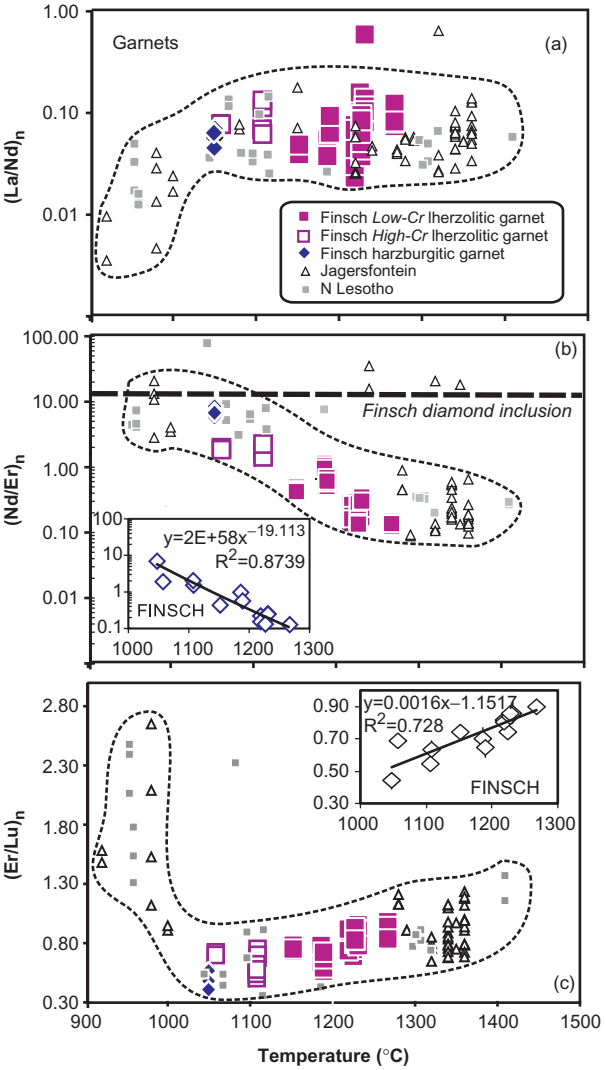

Fig. 15. Plot of xenolith equilibration temperature vs chondrite-normalized REE ratios in Finsch garnets. Temperatures were calculated iteratively using the parameterizations of Brey & Kohler (1990) and O'Neill & Wood (1979). (a) shows a strongly incompatible/moderately incompatible element ratio, $[La/Nd]_n$; (b) an incompatible/compatible element ratio, $[Nd/Er]_n$; (c) a compatible/compatible element ratio, $[Eu/Lu]_n$. These ratios were chosen to highlight the degree of sinuosity in chondrite-normalized garnet REE patterns. Graphs shown as insets in (b) and (c) show lines of best fit and corresponding equations for Finsch garnets. Data sources: Tables 2 and 3; Supplementary Dataset; Shimizu & Richardson (1987); Burgess & Harte (2004); S. A. Gibson *et al.* (unpublished data for northern Lesotho). Normalization factors are from McDonough & Sun (1995).

What might be more important is the amount of garnet that fractionates from the melt because $D_{HREE}^{Grt-melt}$ values vary between one and 10. As the amount of garnet crystallization from the metasomatic melt increases so does the HREE fractionation both in the melt and in the garnets that are in equilibrium with it. Hence garnets that equilibrate at low temperatures with percolating and

Table 5: Comparison of reconstructed whole-rock compositions of Finsch xenoliths with a Low-T and fertile peridotite

	Low-Cr garnet lherzolite							High-Cr garnet lherzolite			Dunite	Harzburgite	Low-*T* peridotite	Fertile peridotite
	BD3692	BD3693	F05JM6	F05JM2	F05JM1	F05JM10	F05JM7	F05JM4	F05BD3694	F05JM8	F05JM5	F05JM9	FRB1402	KR-4003
SiO_2	46·29	45·42	43·93	43·68	42·90	43·31	44·04	47·25	44·11	43·83	41·53	42·62	44·66	44·90
TiO_2	0·04	0·03	0·03	0·05	0·02	0·04	0·03	0·02	0·01	0·01	0·03	0·02	0·03	0·16
Al_2O_3	1·03	1·18	1·36	1·80	0·72	0·96	0·79	1·23	0·47	0·55	0·52	0·18	0·95	4·26
Cr_2O_3	0·24	0·28	0·33	0·37	0·30	0·31	0·28	0·43	0·28	0·34	0·63	0·20		0·41
FeO	6·95	7·12	7·49	8·25	8·44	7·63	7·94	6·71	7·06	6·67	8·17	7·22	6·72	8·02
MnO	0·12	0·10	0·12	0·13	0·12	0·12	0·14	0·11	0·10	0·10	0·12	0·10	0·09	0·13
MgO	44·38	44·93	45·30	44·57	46·85	46·46	46·41	43·05	47·44	47·68	48·81	49·75	46·61	38·12
NiO	0·31	0·33	0·32	0·32	0·35	0·35	0·31	0·26	0·34	0·33	0·36	0·38		0·24
CaO	0·88	1·07	1·29	0·90	0·45	0·77	0·49	0·78	0·28	0·31	0·36	0·11	0·31	3·45
Na_2O	0·12	0·16	0·09	0·07	0·04	0·08	0·06	0·08	0·05	0·02	0·03	0·03	0·09	0·22
K_2O	0·001	0·002	0·004	0·001	0·001	0·001							0·06	0·09
Sc	3·00	7·81	5·82	9·43	3·93	7·93	7·43	10·53	2·51	2·51	7·96	5·63		
Sr	0·85	1·26	1·06	1·78	0·81	0·92	0·77	3·36	0·10	0·39	1·50	0·18		
Zr	0·85	1·26	1·06	1·78	0·81	0·92	0·77	3·36	0·10	0·39	1·50	0·18		
La	0·220	0·363	0·176	0·031	0·022	0·039	0·039	0·053	0·002	0·003	0·005	0·001		
Ce	0·652	1·051	0·531	0·116	0·071	0·145	0·169	0·231	0·020	0·032	0·051	0·018		
Pr	0·077	0·119	0·055	0·020	0·013	0·027	0·025	0·037	0·005	0·008	0·016	0·005		
Nd	0·294	0·374	0·209	0·121	0·069	0·145	0·115	0·179	0·037	0·049	0·134	0·038		
Sm	0·064	0·083	0·052	0·069	0·020	0·053	0·028	0·049	0·010	0·017	0·065	0·008		
Eu	0·025	0·030	0·019	0·030	0·006	0·020	0·011	0·020	0·003	0·006	0·025	0·002		
Gd	0·088	0·104	0·072	0·103	0·023	0·067	0·038	0·068	0·009	0·017	0·069	0·006		
Tb	0·014	0·019	0·013	0·020	0·004	0·011	0·007	0·010	0·001	0·003	0·009	0·001		
Dy	0·102	0·120	0·103	0·145	0·030	0·082	0·050	0·057	0·010	0·018	0·048	0·003		
Ho	0·023	0·029	0·025	0·033	0·006	0·017	0·010	0·011	0·002	0·003	0·009	0·001		
Er	0·071	0·092	0·082	0·102	0·019	0·051	0·030	0·023	0·007	0·011	0·025	0·002		
Tm	0·011	0·014	0·014	0·017	0·004	0·007	0·004	0·003	0·002	0·002	0·004	0·000		
Yb	0·078	0·094	0·096	0·116	0·028	0·058	0·033	0·028	0·011	0·013	0·030	0·003		
Lu	0·012	0·015	0·016	0·019	0·005	0·009	0·005	0·005	0·002	0·003	0·005	0·001		
Mg-no.	91·74	91·65	91·32	90·41	90·64	91·37	91·06	91·77	92·11	92·53	91·23	92·28	92·32	89·26

Mg-number = Mg/(Mg + Fe) × 100 and assumes that all Fe is present as FeO. Data for FRB1402 and KR-4003 are from Boyd *et al.* (1993) and Walter (1998), respectively. Whole-rock compositions were reconstructed using modal analyses from Table 1 and mineral analyses presented in Table 2.

crystallizing metasomatic melts may have relatively fractionated HREE ratios. This is consistent with evidence from LREE that the sub-calcic garnets in the Finsch harzburgite xenoliths have undergone some metasomatism.

EVOLUTION OF THE LITHOSPHERIC MANTLE BENEATH THE WESTERN MARGIN OF THE KAAPVAAL CRATON

We have reconstructed the bulk-rock compositions of the Finsch xenoliths by combining estimates of modal mineralogy with major- and trace-element mineral chemistry (Table 5). This type of bulk-rock reconstruction is sensitive to any heterogeneity in modal mineralogy but was chosen in preference to bulk-rock analysis because it overcomes: (1) secondary metasomatic effects related to infiltration of kimberlite melt (e.g. Hawkesworth *et al.*, 1983; Simon *et al.*, 2007); (2) hydrothermal alteration and serpentinization, which causes loss of K, Rb, etc. and introduction of FeO, CaO, TiO_2 (Boyd *et al.*, 1997) and SiO_2. As might be expected from their variations in modal mineralogy and mineral chemistry, the Finsch xenoliths exhibit a wide range of bulk-rock compositions. The harzburgites have the lowest concentrations of CaO, Al_2O_3, FeO, TiO_2 and LREE, and are the most 'depleted' (e.g. Fig. 16).

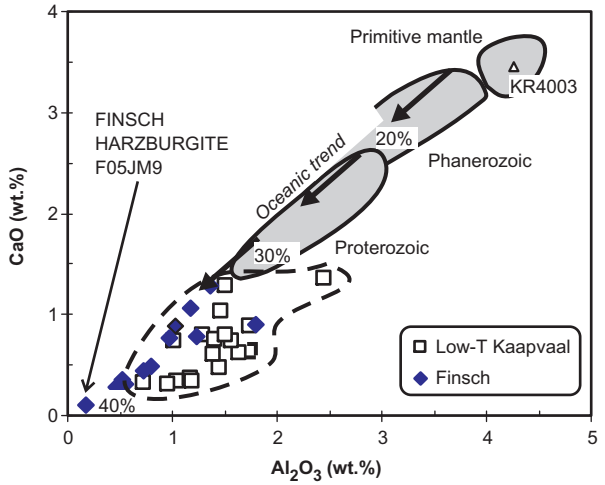

Fig. 16. Bulk-rock Al_2O_3 vs CaO plot to show the refractory nature of some Finsch mantle xenoliths. Estimates of the compositions of residues that would be generated as a result of 20, 30 or 40% adiabatic decompression melting of a 'parcel' of mantle that intersected the solidus at 5 GPa are from Herzberg (2004). The 'oceanic trend', shown by bold arrows, is from Boyd (1989). Data sources: Table 5; Xue *et al.* (1990); Boyd *et al.* (1993); O'Reilly *et al.* (2001).

Concentrations of these magmaphile oxides and elements are greatest in the lherzolites, especially BD3692 and BD3693, but are less than those present in fertile mantle (Table 5).

Melt depletion: formation of Finsch harzburgites

Finsch garnet harzburgite F05JM9 is characterized by high bulk-rock Mg-number (0·923), moderate FeO (7·22 wt %), and low SiO_2 (42·6 wt %), Al_2O_3 (0·18 wt %) and CaO (0·11 wt %; Table 5) relative to fertile mantle peridotite. Herzberg (2004) has recently parameterized the results of experimental studies on fertile peridotite to calculate the compositions of residues that form during polybaric melting of upwelling mantle (Fig. 17). A comparison of the estimated abundances of Al_2O_3, SiO_2, FeO and MgO in the Finsch harzburgite with the melt trajectories calculated by Herzberg (2004) indicates that F05JM9 may represent the residue of extensive (~40%), polybaric melting of fertile peridotite (Fig. 17). Figure 17 suggests that in upwelling convecting mantle such large-degree melting would start at 4·5 GPa and continue until 1·5 GPa. The high-pressure melts would be in equilibrium with garnet whereas at the top of the melting column spinel would be the stable aluminous phase, although it is likely that most of this would have been exhausted at such large degrees of partial melting. If we assume that the upwelling mantle had a composition similar to a fertile peridotite, such as KR4003, then intersection of the solidus at 4·5 GPa corresponds to a potential temperature (T_p) of ~1550°C (Fig. 18). During the Archaean, such a T_p would have

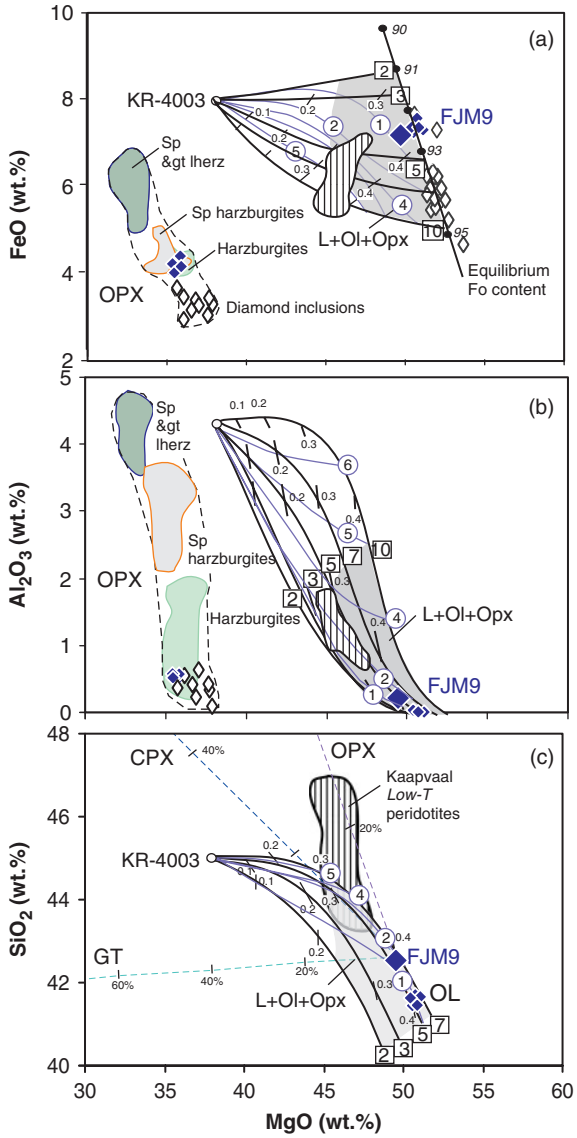

Fig. 17. Calculated compositions of residues generated by fractional melting of fertile peridotite KR-4003 (Herzberg, 2004). Continuous lines show the compositional change of the residue at a range of initial (numbers in open squares) and final (numbers in open circles) melting pressures (GPa). The shaded field, labelled L + Ol + Opx, corresponds to the predicted compositions of harzburgite residues. Tick marks correspond to the degree of partial melting. The composition of F05JM9 (large filled diamond) plots close to the estimated trajectory of a residue that underwent initial melting at 5 GPa and final melting at 1·5 GPa. The field of Low-*T* Kaapvaal peridotites (striped ornament) is shown for comparison. The compositions of orthopyroxene in mantle peridotites are also shown in (a) and (b) to illustrate the range of FeO and Al_2O_3 contents in xenoliths with different bulk-rock compositions. Small-open and small-filled diamonds show compositions of olivine and orthopyroxene in Finsch diamond inclusions and Finsch harzburgite, respectively. Dashed lines in (c) indicate the effects on bulk-rock MgO and SiO_2 of adding different percentages of orthopyroxene, clinopyroxene and garnet. Data sources: Hervig *et al.* (1980); Cox *et al.* (1987); Xue *et al.* (1990); Boyd *et al.* (1993); Ionov *et al.* (1993); Bernstein *et al.* (1998); Walter (1998); Griffin *et al.* (2004).

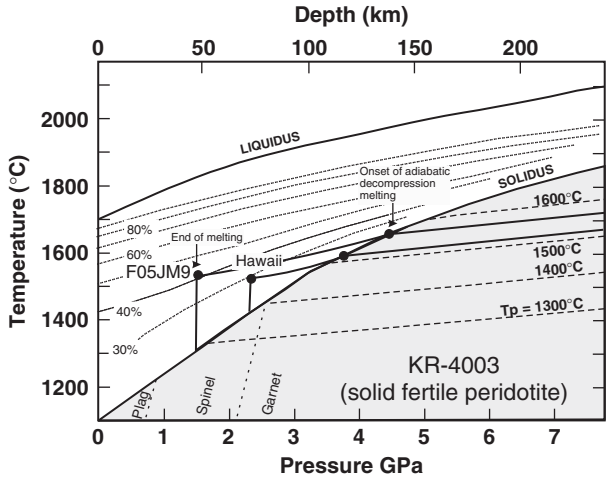

Fig. 18. Pressure (and depth) vs temperature plot to show the schematic trajectory of the melt that was extracted to form harzburgite F05JM9. Adiabatic decompression melting of anhydrous fertile peridotite (KR4003) between ~ 5 and 1·5 GPa would generate a residue with a similar composition to F05JM9 (Fig. 15). This corresponds to a mantle potential temperature (T_p) of ~1550°C and shows that, at the time of melt cessation, the residue would be in the spinel stability field. The gradient of the mantle adiabat is assumed to be 0·6°C/km (McKenzie & Bickle, 1989). The trajectory of a Hawaiian picritic melt is shown for comparison (Thompson & Gibson, 2000; Herzberg & O'Hara, 2002).

been similar to that of ambient convecting mantle (Richter, 1988) and does not support hypotheses that invoke harzburgites as residues of high-pressure and -temperature melting in upwelling mantle plumes (Pearson *et al.*, 1995*a*; Herzberg, 1999; and see below).

The extremely low contents of CaO in garnet (<1·42 wt %) and Al_2O_3 in orthopyroxene (<0·66 wt %), together with the high Mg-number of olivine and orthopyroxene (up to 95·5) in Finsch diamond inclusions (Gurney *et al.*, 1979; Tsai *et al.*, 1979; Richardson *et al.*, 1984), indicate that the lithospheric mantle beneath the western Kaapvaal may have undergone even larger amounts of melting than we have estimated for harzburgite F05JM9. The diamond inclusions would have been shielded from any post 3·3 Ga melt enrichment events and it may be that harzburgite F05JM9 has undergone slight modification by cryptic metasomatism, post diamond formation as discussed above. Re–Os ages, determined on whole-rock samples and sulphide inclusions from both lherzolitic and harzburgitic Finsch xenoliths, confirm that this melt depletion event occurred prior to ~3 Ga (Pearson *et al.*, 1995*a*; Griffin *et al.*, 2004).

We used the following equation to calculate the concentration of elements in the aggregate fractional melt that generated a residue with the composition of the Finsch harzburgite:

$$C_o = FC_l + (1 - F)C_s$$

where C_o is the concentration in the original mantle source (which we have assumed to be similar to KR4003; Walter, 1998), F is the mass fraction of the aggregate melt, C_l is the concentration in the aggregate melt and C_s is the concentration in the solid residue (i.e. F05JM9, Table 5). Because the amount of melting we have estimated from harzburgite F05JM9 is a minimum, estimates of the composition of the extracted melt will contain less MgO but be richer in CaO and Al_2O_3 than the actual melts. Our calculations suggest that the aggregate melt, which left F05JM9 as a final residue, contained ~20 wt % MgO, 9·5 wt % FeO, 9·66 wt % CaO, 11·84 wt % Al_2O_3 and 49 wt % SiO_2. This is similar to a Hawaiian picrite, although subtle differences in some oxides (e.g. Al_2O_3) reflect the shallower top of the melt column and slightly higher T_p involved in the formation of the Finsch residue. We envisage that the residue formed in an Archaean spreading-ridge environment.

The most plausible explanation for the origin of the high Cr-number, sub-calcic garnets present both in Finsch diamond inclusions and peridotite xenoliths (e.g. F05JM9) is that they formed during lithospheric thickening, rather than that they are residual phases of an early melting event (i.e. they are metamorphic). In rare peridotite xenoliths, pyrope garnet can be seen exsolving from orthopyroxene (Cox *et al.*, 1987; Dawson, 2004) but these garnets are characterized by low Cr_2O_3 contents (~2·5 wt %) and thus unlike the ones that occur in the Finsch harzburgites. Previous studies have shown that high-Cr pyrope garnets must have formed from a melt residue with a high Cr-number (>30). Because the $K_d Cr/Al^{Grt-melt}$ value is ~1 (Canil & Wei, 1992), residues with such high Cr-number are not able to form as a result of melting in the garnet stability field (Stachel *et al.*, 1998). Melt depletion in the spinel stability field can, however, produce a residue with a Cr-number as high as 42 (Tainton & McKenzie, 1994). The wide variation of garnet Cr contents might indicate variable modal amounts of Cr spinel in the original melt residue, although we believe that, in general, the modal amount of Cr-spinel would be low, such that only a small amount of garnet would form. Such pressure-induced transformation of the aluminous phase would theoretically also consume two pyroxenes and produce mantle rich in olivine and low in orthopyroxene (Johnson *et al.*, 1990):

$$2 \cdot 5MgSiO_3 + MgAl_2O_4 + 0 \cdot 75CaMgSi_2O_6 = Mg_2SiO_4 + Ca_{0\cdot75}Mg_{2\cdot25}Al_2Si_3O_{12}.$$

orthopyroxene + spinel + clinopyroxene = olivine + garnet

Clinopyroxene would not, however, be present in a residue generated by very high degrees of partial melting (see above) and this would limit the amount of Ca available for partitioning into garnet during cratonization.

This would explain the very low Ca contents of the pyrope garnets in the Finsch diamond inclusions (Fig. 2); the compositions of some of these may be represented by the reaction

$$4Fe_{0\cdot05}Mg_{0\cdot95}SiO_3 + Fe_{0\cdot27}Mg_{0\cdot73}Cr_{0\cdot7}Al_{1\cdot3}O_4 + 0\cdot05CaFe_{0\cdot1}Mg_{0\cdot9}Si_2O_6 =$$

$$\text{orthopyroxene} + \text{spinel} + \text{clinopyroxene}$$

$$Fe_{0\cdot12}Mg_{1\cdot88}SiO_4 + Ca_{0\cdot05}Fe_{0\cdot36}Mg_{2\cdot67}Cr_{0\cdot7}Al_{1\cdot3}Si_3O_{12}.$$

$$\text{olivine} + \text{Low-Ca pyrope garnet}$$

Spinel harzburgite would also have very low concentrations of REE and this would further limit REE partitioning into the sub-calcic garnets and explain the extremely low (sub-chondritic) abundances of REE in the harzburgites (Table 5).

Significance of Low-*T* Finsch peridotites

The Kaapvaal lithospheric mantle is believed to predominantly consist of Mg- and enstatite-rich (20–45%), coarse garnet peridotites that last equilibrated at low temperatures (below 1150°C); these have been termed Low-*T* peridotites (Boyd & Mertzman, 1987; Boyd, 1989). Samples of Low-*T* peridotites from the Kaapvaal and Siberian cratons have been noted for their high Mg-number at a given modal olivine content relative to samples from oceanic lithosphere (abyssal peridotites and ophiolite tectonites; Fig. 19). The high Mg-number of Low-*T* cratonic peridotites has been widely attributed to their origin as residues of very high amounts of partial melting, as a consequence of elevated Archaean mantle temperatures (Boyd, 1989). The Low-*T* Finsch peridotites are significant because they have much higher modal olivine (up to 96%) than has previously been estimated for Low-*T* peridotites (<85%) from other parts of the Kaapvaal craton (Hawkesworth *et al.*, 1983; Boyd & Mertzman, 1987; Boyd *et al.*, 1997; Grégoire *et al.*, 2003; Simon *et al.*, 2007). Nevertheless, Low-*T* peridotites with very high modal olivine contents (up to 98·5 modal %) have recently been discovered from the Greenland and Slave cratons (Bernstein *et al.*, 1998; Schmidberger & Francis, 1999). These are similar to the Finsch Low-*T* peridotites although, with the exception of the garnet harzburgite (F05JM09), the Finsch samples have slightly less Mg-rich olivine at a given modal per cent olivine (Fig. 19).

The high modal olivine content of the Finsch Low-*T* peridotites is compensated by low modal orthopyroxene (<17%). Other Kaapvaal (and also Siberian) craton Low-*T* peridotites have an average of ~30% orthopyroxene (Boyd, 1989). This is higher than has been observed in residues of partial melting experiments of anhydrous fertile peridotites (<25%; e.g. Walter, 1998), and in numerical models of polybaric mantle melting of anhydrous peridotites (Herzberg, 2004).

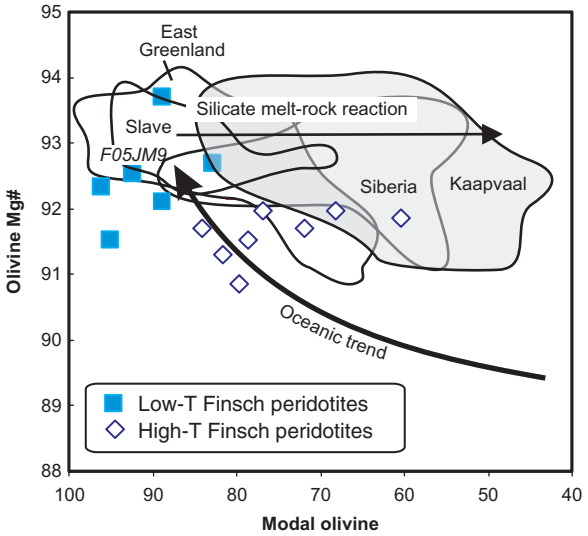

Fig. 19. Plot of modal per cent olivine vs olivine Mg-number ([Mg/(Mg + Fe)] × 100) after Boyd (1989) for Low-*T* Finsch peridotites (filled squares) and higher temperature Finsch peridotites (open diamonds). It should be noted that, unlike other xenoliths from the Kaapvaal craton, some of those from Finsch plot at the high Mg-number end of the 'oceanic trend' of Boyd (1989). Data sources: Tables 1 and 2; Hawkesworth *et al.* (1983); Boyd & Mertzman (1987); Boyd (1989); Boyd *et al.* (1997); Bernstein *et al.* (1998); Schmidberger & Francis (1999); Grégoire *et al.* (2003); Simon *et al.* (2007).

The large variation in modal olivine (40–85%) and high contents of orthopyroxene in Low-*T* Kaapvaal peridotites have been attributed to: (1) large-degree melting of peridotite at high pressures (Boyd, 1989; Herzberg, 1999); (2) metamorphic differentiation (Boyd, 1989); (3) coarse layering in the lithospheric mantle as a result of cumulate sorting (Herzberg, 1993); (4) metasomatic replacement of olivine by orthopyroxene (Boyd *et al.*, 1993; Kelemen *et al.*, 1998). In contrast, the unusually low modal orthopyroxene contents of the Finsch Low-*T* peridotites are consistent with those calculated for residues of melt extraction.

We believe that the Low-*T* Finsch peridotites are important end-members in models of the multi-stage evolution of the Kaapvaal lithospheric mantle. Figure 17 shows that, if the bulk-rock composition of Finsch harzburgite (F05JM9) is representative of the initial Kaapvaal lithospheric mantle residue, the increase in modal orthopyroxene evident in other Low-*T* peridotites may be associated with an increase of up to ~4 wt % SiO_2. A simple increase in modal orthopyroxene with a composition similar to that present in the Kaapvaal Low-*T* peridotites (as a result of SiO_2 addition) does not, however, satisfactorily account for either the elevated contents of Al_2O_3 (0·7–2·46 wt %) and CaO (0·31–1·36 wt %) of these xenoliths relative to the Finsch harzburgite (0·18 wt % Al_2O_3 and 0·11 wt % CaO; Fig. 16) or the depletion in FeO and MgO. The Al_2O_3

contents of the orthopyroxene in the Kaapvaal Low-T peridotites are similar to those at Finsch (<0·8 wt %), presumably because they equilibrated along similar geothermal gradients in the garnet stability field. The increase in Al_2O_3 of the Kaapvaal Low-T peridotites may be due to either addition of orthopyroxene that originally contained ~4 wt % Al_2O_3 [i.e. similar to the composition of orthopyroxene in equilibrium with spinel rather than garnet peridotite (Fig. 17b)] or introduction of additional phases, such as spinel, garnet and/or phlogopite (Bell *et al.*, 2003).

MELT–ROCK REACTION: METASOMATISM AND LHERZOLITE FORMATION

The role of metasomatic melts vs fluids involved in the LREE enrichment of sub-calcic garnets remains controversial (e.g. Stachel & Harris, 1997; Burgess & Harte, 2004; Stachel *et al.*, 2004). Stachel and co-workers have argued against the role of melts on the grounds that they would freeze upon equilibration with the surrounding peridotite and have proposed, instead, that the high LREE, and low Ti, Zr, Y and HREE that characterize sub-calcic garnets are related to a C–H–O-rich fluid. For H_2O-rich fluids, interconnectivity along grain boundaries is increased considerably with increasing temperature and pressure (Watson *et al.*, 1990) and Stachel & Harris (1997) have argued that metasomatism of sheared peridotites, within the diamond stability field, could take place at subsolidus conditions by H_2O-rich fluids. Nevertheless, experiments by Ono *et al.* (2002) have indicated that dihedral angles for aqueous fluids are only <60° at pressures greater than 8–9 GPa. Percolation of fluids would therefore occur only at pressures greater than those observed in the lithospheric mantle. The experiments of Ono *et al.* (2002) involved a pyrope-rich matrix and may not be wholly appropriate for peridotites. Nevertheless, the low equilibration pressures (3·5 GPa) that we have estimated for the Finsch harzburgites and their coarse–equant textures do not appear to be conducive to the percolation of fluids. We therefore currently favour a mechanism involving metasomatic melts to explain the trace-element characteristics of sub-calcic Finsch garnets. We believe that the migration of these melts through the lithospheric mantle would be enhanced if they are volatile-rich and are of such a large volume that they would not fully react with the surrounding peridotite. Our model implies that this metasomatism is not directly linked to Finsch diamond formation.

The wide variations in bulk-rock composition that we have observed in the Finsch peridotite xenolith suite appear to be the result of different degrees of metasomatism of a harzburgite host. Our results indicate that, prior to ~120 Ma, the lithosphere beneath the western part of the Kaapvaal craton had been pervasively metasomatized between 180 and 130 km depth (Fig. 10). Lherzolites from the base of the lithospheric mantle (e.g. BD3692, F05JM6) appear to have undergone significant enrichment in Fe, Ca, Al, Si, Mn, Na, Ti, Cr, REE, Sr, Y and Zr relative to the 'shallow' harzburgites. The style of modal metasomatism beneath Finsch also varies with depth: both Cr-diopside and garnet (G9) are present at depths >130 km but Cr diopside is absent between 100 and 130 km. The continuous Ca vs Cr trends that we have observed in the Finsch garnets have been reported from other mantle xenolith suites and interpreted as evidence either of progressive major-element depletion such that high-Cr sub-calcic garnets (i.e. G10 garnets) found in harzburgites are residua of melt extraction from primary lherzolite compositions (Griffin *et al.*, 1992; Grütter *et al.*, 1999), or of refertilization of harzburgites to form lherzolites (Schulze, 1991; Griffin *et al.*, 1999*a*; Burgess & Harte, 2004).

Metasomatic melt compositions

Previous studies have highlighted the fact that Cr-diopsides and pyrope garnets in the same mantle xenolith appear to have crystallized from melts of different compositions (e.g. Jones, 1987; Simon *et al.*, 2003). In some cases, this may be an artefact of errors in garnet–melt partition coefficients (Tainton & McKenzie, 1994). We have used the $D^{Grt-melt}$ and $D^{Cpx-melt}$ values defined in Table 4 to calculate equilibrium melt compositions responsible for lithospheric mantle enrichment and lherzolite formation beneath Finsch. Mantle-normalized compositions of these melts are plotted in Fig. 20. This shows that the estimated compositions of the equilibrium melts are extremely similar for both the Cr-diopsides and pyrope garnets present in lherzolite F05JM7. The metasomatic melts are strongly enriched in LREE (up to 500 × primitive mantle) and large ion lithophile elements (LILE) and have depletions at Th, Nb and Ti on mantle-normalized multi-element plots. The LREE/HREE ratios of the melts appear to increase with decreasing equilibration pressure such that the compositions of melts estimated to be in equilibrium with garnets in the diamond inclusions, High-Cr lherzolitic and sub-calcic harzburgitic garnets have much steeper normalized LREE/HREE patterns than those of the Low-Cr lherzolitic garnets. When normalized to the composition of melts in equilibrium with the least enriched xenolith (F05JM9) it can be seen that the greatest enrichments in the high-pressure lherzolites are in the LREE, HREE, Zr, Sr and perhaps Ti (Figs 21 and 22). The most plausible interpretation of this difference in equilibrium melt compositions is that the melts have undergone fractional crystallization of both garnet and clinopyroxene during their ascent. Garnets, and where present Cr-diopsides, record evidence of this melt–rock reaction in single xenoliths. A similar percolation fractionation model was proposed by Burgess & Harte (2004) to account for

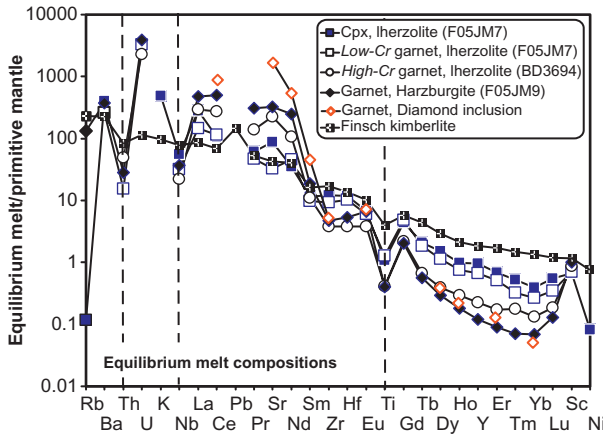

Fig. 20. Primitive-mantle-normalized trace-element concentrations of melts estimated to be in equilibrium with garnet and clinopyroxene present in Finsch xenoliths and a garnet from a diamond inclusion (Shimizu & Richardson, 1987). Melt compositions were calculated using $D^{Grt-melt}$ and $D^{Cpx-melt}$ values from Table 4 and mineral analyses presented in Table 2 and the Supplementary Dataset. The primitive-mantle-normalized multi-element pattern of a Finsch Group II kimberlite (Becker & Le Roex, 2006) is shown for comparison. Normalization factors are from McDonough & Sun (1995).

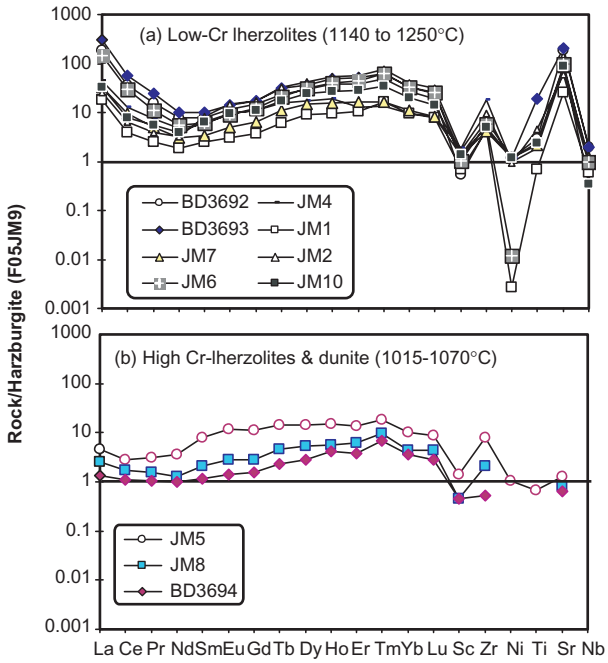

Fig. 21. Reconstructed whole-rock trace-element concentrations of (a) high-temperature and (b) low-temperature Finsch lherzolites relative to highly refractory Finsch harzburgite F05JM9. Temperatures were calculated using the two-pyroxene solvus and the olivine–garnet Fe–Mg exchange geothermometers of Brey & Kohler (1990) and O'Neill & Wood (1979), respectively (Table 3). Whole-rock concentrations are from Table 5.

variations in garnet chemistry in Jagersfontein peridotite xenoliths.

Age of lithospheric enrichment events

Richardson *et al.* (1984) have proposed that the Sr-isotopic ratios of sub-calcic garnet inclusions from Finsch diamonds required a two-stage melting model, involving melt depletion and enrichment (immediately prior to 3·3 Ga diamond formation). Concentrate sub-calcic garnets (i.e. harzburgite paragenesis) from Finsch have higher $^{143}Nd/^{144}Nd$ (0·5112–0·512) and $^{87}Sr/^{86}Sr$ ratios (0·707–0·732) than garnet inclusions in diamond (0·5109, 0·7035; Richardson *et al.* 1984). $^{143}Nd/^{144}Nd$ and $^{87}Sr/^{86}Sr$ ratios for a Low-Cr lherzolitic garnet are even higher (0·51295 and 0·7638; Pearson *et al.*, 1995*a*). Sm–Nd model ages are slightly younger for the concentrate sub-calcic garnets (t_{CHUR} = 1·3–3·1 Ga) than the diamond inclusions but even younger for the lherzolitic garnet (t_{CHUR} = 181 Ma). Ages of the latter are very close to the time of entrainment and emplacement of the Finsch kimberlite. The Sm–Nd model ages and wide range of $^{87}Sr/^{86}Sr$ ratios indicate that lithospheric enrichment, of variable styles, has occurred both before and after 3·3 Ga diamond formation beneath the western margin of the Kaapvaal craton. Sm–Nd model ages for diopsides suggest that the Kaapvaal lithospheric mantle was subjected to a major metasomatic event at 1 Ga (Pearson, 1999) but if we assume that the Sm–Nd model age for the Low-Cr lherzolitic garnet analysed by Pearson *et al.* (1995*a*) is representative of this paragenesis, then significant refertilization of the base of the western Kaapvaal lithosphere may have occurred more recently.

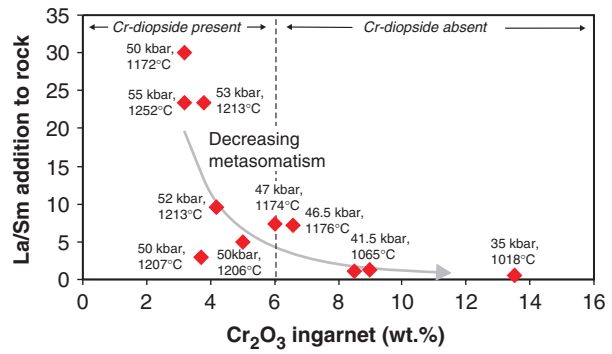

Fig. 22. Variation of garnet Cr_2O_3 content with the degree of LREE enrichment (expressed by La/Sm ratio) experienced by the whole-rock. La/Sm ratios for all samples were normalized to those in garnet from Finsch harzburgite F05JM9 to calculate the amount of addition. Pressures and temperatures were calculated using the two-pyroxene solvus geothermometer of Brey & Kohler (1990), the olivine–garnet Fe–Mg exchange thermometer of O'Neill & Wood (1979), the Al-in-opx barometer of Brey *et al.* (2008). Data are from Tables 2, 3 and 5.

We note that the predicted compositions of metasomatic melts in equilibrium with the clinopyroxene-free samples have much higher concentrations of LREE and lower concentrations of Ti and HREE than the host 120 Ma Finsch kimberlite (Fig. 20). Those in equilibrium with the

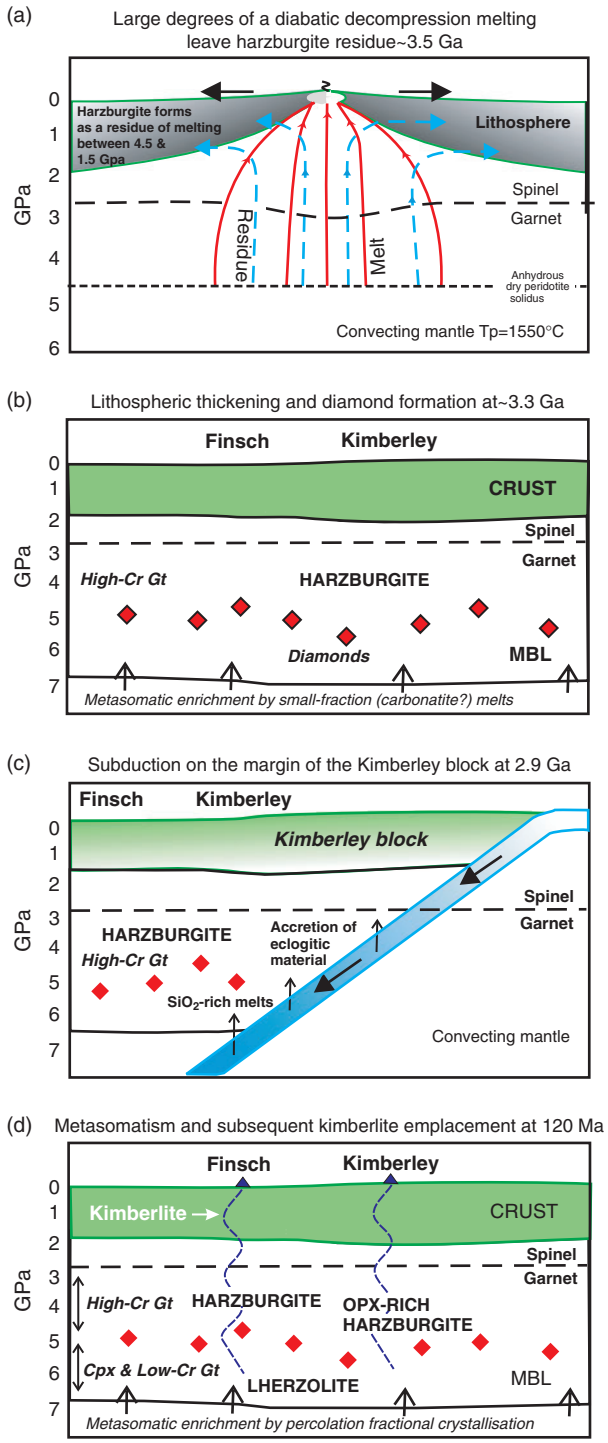

Fig. 23. Schematic illustration of the melt depletion and enrichment events in the lithospheric mantle beneath the western Kaapvaal craton. (a) A comparison of the reconstructed bulk-rock compositions of Finsch harzburgites with experimental data suggests that they may represent residues of large amounts (~40%) of adiabatic decompression melting between 5 and 1·5 GPa, at a mantle potential temperature of 1550°C. That temperature would have been similar to that of ambient Archaean mantle (Richter, 1988). Peridotitic garnets included in diamonds from both Finsch and Kimberley have Nd model ages of 3·2–3·3 Ga but are thought to have been derived from a source ~300 Myr older (Richardson *et al.*, 1984). (b) These Nd model ages are believed to mark the time of stabilization of part of the cratonic nuclei (de Wit *et al.*, 1992) although much of this may have occurred later, in Neoarchaean times (Pearson, 1999; Pearson *et al.*, 2002). The chemistry of sub-calcic garnets indicates that prior to diamond formation, the lithospheric mantle had been subjected to enrichment in LREE and LILE (this study, Richardson *et al.*, 1984; Shimizu & Richardson, 1987). (c) Major addition of subduction-related eclogite, by tectonic imbrication or magmatic underplating, is thought to have occurred on the eastern margin of the Kimberley block in the Late Archaean (2·9 Ga; Richardson *et al.*, 2001). Eclogitic garnets in Finsch diamond inclusions give much younger (Proterozoic) ages (Smith *et al.*, 1991). Late Archaean subduction may also be responsible for genesis of silica-rich melts that have reacted with olivine in the overlying lithospheric mantle to form orthopyroxene-rich harzburgites sampled at Kimberley (Bell *et al.*, 2005); at Finsch the harzburgites resemble residues that form in partial melting experiments on fertile peridotite and these appear to represent a close approximation to the composition of the early Archaean lithospheric mantle. (d) The presence of low-Cr pyrope garnet and Cr-diopside in Finsch lherzolites, which last equilibrated at pressures >5 GPa, is evidence of 'refertilization' of the base of the mechanical boundary layer. Equilibrium melt compositions calculated for both phases are almost identical and indicate their crystallization from small fraction melts, different in composition to the host kimberlite. Both the low-Cr pyrope garnet and Cr-diopside are chemically homogeneous, suggesting that they formed prior to entrainment.

lherzolites are more comparable. Nevertheless, variations in garnet and clinopyroxene chemistry and modal abundance of the peridotites must have occurred prior to entrainment and ascent to the surface, otherwise more evidence of textural and chemical disequilibrium would be apparent. In this respect, the metasomatic enrichment that we have identified at Finsch is distinctly different from that which caused the formation of strongly zoned garnets found in xenoliths entrained by the 90 Ma, Group 1, Jagersfontein kimberlite (Burgess & Harte, 2004). Differences between lithospheric mantle sampled by Group I and II southern African kimberlites from the SW of the Kaapvaal craton have previously been proposed by Griffin *et al.* (1999*b*, 2003). They suggested, from their study based predominantly on garnet concentrates, that Group II kimberlites sample less metasomatized lithospheric mantle than Group I kimberlites. Our findings for Finsch are broadly consistent with this hypothesis.

CONCLUSIONS

(1) Mantle peridotite xenoliths from Finsch Mine provide a rare insight into the evolution of the lithosphere beneath the west of the Kaapvaal craton. They are important because they were entrained by Group II kimberlites and have not been subjected to the metasomatic event that is evident in mantle xenoliths entrained by Group I kimberlites (e.g. Jagersfontein, Wesselton, NW Lesotho). This recent metasomatism appears to have caused major- and trace-element disequilibrium in lithospheric mantle phases, such as garnet and clinopyroxene

(Griffin *et al.*, 1999*b*; Simon *et al.*, 2003; Burgess & Harte, 2004; S. A. Gibson *et al.*, unpublished data).

(2) Our study shows that the amount of Cr-diopside present in the sub-Finsch lithospheric mantle decreases consistently with decreasing depth. We interpret this as evidence of reduced amounts of mantle metasomatism as low-volume small-fraction volatile-rich melts 'froze' during their ascent through the lithospheric mantle. As has been observed from other parts of the Kaapvaal craton, the deepest samples from Finsch are all garnet lherzolites whereas garnet harzburgites were entrained from shallower depths. Pressure estimates using the Al-in-Opx barometer of Brey *et al.* (2008) place the lherzolite–harzburgite transition at ~35–40 kbar.

(3) Variations in incompatible trace elements in garnet and clinopyroxene from lherzolite xenoliths correlate with those of major elements, such as Ca. However, this correlation is not apparent in the harzburgitic garnets, where Ca contents are low and concentrations of LREE are high. The REE patterns of the garnets exhibit a systematic variation from 'smooth' to 'sinusoidal' with increasing Cr/Ca ratio. The variation in LREE may be due to changes in crystal chemistry related to variations in pressure (and temperature) and/or accompanying differences in bulk-rock composition. The latter may reflect decreasing amounts of mantle metasomatism with depth.

(4) The unusually low modal abundances of orthopyroxene in the Finsch peridotites, compared with those from elsewhere in the Kaapvaal craton, suggest that this part of the lithosphere has not undergone the pervasive SiO_2 enrichment experienced further east. The reaction of silica-rich melt with olivine to form orthopyroxene is believed to have occurred at ~2·9 Ga and has been linked with subduction zones, associated with the amalgamation of the Kimberley and Witwatersrand blocks, and stabilization of the Kaapvaal craton (e.g. Schmitz *et al.*, 2004; Simon *et al.*, 2007). This silica enrichment has also been linked by some to diamond formation (Bell *et al.*, 2005). In contrast, the low modal orthopyroxene contents in the diamondiferous Finsch peridotites (Shee *et al.*, 1982; Viljoen *et al.*, 1992) suggest that these processes are independent of one another. The sub-Finsch lithospheric mantle would have been remote from the subduction zone on the eastern margin of the Kimberley block and this may explain the lower modal amounts of orthopyroxene. The lithospheric mantle sampled by the Kimberley kimberlites (Fig. 23) would have been much closer to the subduction zone and hence more susceptible to modification by slab-derived melts and/or fluids. We believe that Finsch harzburgite F05JM9 represents one of the most highly refractory xenoliths sampled from the Kaapvaal craton.

ACKNOWLEDGEMENTS

We are extremely grateful to Mathew Field, William MacDonald, Jock Robey and Ken Tainton of DeBeers Consolidated Mines who granted permission to sample the xenoliths at Finsch Mine and provided logistical support to J.M. We thank Barry Dawson for his encouragement and for generously donating his collection of Finsch mantle xenoliths. Chris Hayward is thanked for his assistance with the electron microprobe, and Dan McKenzie for allowing us to use his PTMIN and FITPLOT software. Research on Finsch xenoliths was initiated by J.M. as an MSc project at the University of Cambridge and was funded by the Department of Earth Sciences. We are indebted to G. Pearson, T. Stachel and K. S. Viljoen for their thorough and constructive reviews of an earlier version of the manuscript. Their thought-provoking comments have greatly improved the paper. A further set of comments was provided by an anonymous reviewer. This is Department of Earth Sciences Contribution ES9309.

SUPPLEMENTARY DATA

Supplementary data for this paper are available at *Journal of Petrology* online.

REFERENCES

Appleyard, C. M., Viljoen, K. S. & Dobbe, R. (2004). A study of eclogitic diamonds and their inclusions from the Finsch kimberlite pipe, South Africa. *Lithos* **77**(1–4), 317–332.

Ballaran, T. B., Carpenter, M. A., Geiger, C. A. & Koziol, A. M. (1999). Local structural heterogeneity in garnet solid solutions. *Physics and Chemistry of Minerals* **26**(7), 554–569.

Becker, M. & Le Roex, A. P. (2006). Geochemistry of South African on- and off-craton, Group I and Group II kimberlites: petrogenesis and source region evolution. *Journal of Petrology* **47**(4), 673–703.

Bell, D. R., Schmitz, M. D. & Janney, P. E. (2003). Mesozoic thermal evolution of the southern African mantle lithosphere. *Lithos* **71**, 273–287.

Bell, D., Grégoire, M., Grove, T., Chatterjee, N., Carlson, R. & Buseck, P. (2005). Silica and volatile-element metasomatism of Archean mantle: a xenolith-scale example from the Kaapvaal Craton. *Contributions to Mineralogy and Petrology* **150**(3), 251–367.

Bernstein, S., Kelemen, P. B. & Brooks, C. K. (1998). Depleted spinel harzburgite xenoliths in Tertiary dykes from East Greenland: Restites from high degree melting. *Earth and Planetary Science Letters* **154**(1–4), 221–235.

Bernstein, S., Hanghøj, K., Kelemen, P. B. & Brooks, C. K. (2006). Ultra-depleted, shallow cratonic mantle beneath West Greenland: dunitic xenoliths from Ubekendt Ejland. *Contributions to Mineralogy and Petrology* **152**(3), 335–347.

Blundy, J. & Wood, B. (1994). Prediction of crystal–melt partition coefficients from elastic moduli. *Nature* **372**(6505), 452–454.

Blundy, J. & Wood, B. (2003). Partitioning of trace elements between crystals and melts. *Earth and Planetary Science Letters* **210**(3–4), 383–397.

Boyd, F. R. (1989). Compositional distinction between oceanic and cratonic lithosphere. *Earth and Planetary Science Letters* **96**(1–2), 15–26.

Boyd, F. R. & Mertzman, S. A. (1987). Composition and structure of the Kaapvaal lithosphere, southern Africa. *Magmatic Processes Physiochemical Principles* **1**, 13–24.

Boyd, F. R., Pearson, D. G., Nixon, P. H. & Mertzman, S. A. (1993). Low-calcium garnet harzburgites from Southern Africa—their relations to craton structure and diamond crystallization. *Contributions to Mineralogy and Petrology* **113**(3), 352–366.

Boyd, F. R., Pokhilenko, N. P., Pearson, D. G., Mertzman, S. A., Sobolev, N. V. & Finger, L. W. (1997). Composition of the Siberian cratonic mantle: evidence from Udachnaya peridotite xenoliths. *Contributions to Mineralogy and Petrology* **128**(2), 228–246.

Brey, G. P. & Kohler, T. (1990). Geothermobarometry in four-phase lherzolites II. New thermobarometers, and practical assessment of existing thermobarometers. *Journal of Petrology* **31**(6), 1353–1378.

Brey, G. P., Kohler, T. & Nickel, K. G. (1990). Geothermobarometry in four-phase lherzolites I. Experimental results from 10 to 60 kb. *Journal of Petrology* **31**, 1313–1352.

Brey, G. P., Bulatov, V. K. & Girnis, A. V. (2008). Geobarometry for peridotites: experiments in simple and natural systems from 6 to 10 GPa. *Journal of Petrology* **49**(1), 3–24.

Brunelli, D., Seyler, M., Cipriani, A., Ottolini, L. & Bonatti, E. (2006). Discontinuous melt extraction and weak refertilization of mantle peridotites at the Vema Lithospheric Section (Mid-Atlantic Ridge). *Journal of Petrology* **47**(4), 745–771.

Burgess, S. R. & Harte, B. (1999). Tracing lithosphere evolution through the analysis of heterogeneous G9/G10 garnets in peridotite xenoliths, l: Major element chemistry. In: Gurney, J. J., Gurney, J. L., Pascoe, M. D. & Richardson, S. H. (eds) *Proceedings of the 7th International Kimberlite Conference*. Cape Town: Red Roof Design, pp. 66–80.

Burgess, S. R. & Harte, B. (2004). Tracing lithosphere evolution through the analysis of heterogeneous G9–G10 garnets in peridotite xenoliths, II: REE chemistry. *Journal of Petrology* **45**(3), 609–634.

Canil, D. & O'Neill, H. S. C. (1996). Distribution of ferric iron in some upper-mantle assemblages. *Journal of Petrology* **37**(3), 609–635.

Canil, D. & Wei, K. (1992). Constraints on the origin of mantle-derived low Ca garnets. *Contributions to Mineralogy and Petrology* **109**, 421–430.

Canil, D., O'Neill, H. S. C., Pearson, D. G., Rudnick, R. L., McDonough, W. F. & Carswell, D. A. (1994). Ferric iron in peridotites and mantle oxidation states. *Earth and Planetary Science Letters* **123**(1–3), 205–220.

Cox, K. G., Smith, M. R. & Beswetherick, S. (1987). Textural studies of garnet lherzolites: evidence of exsolution origin from high-temperature harzburgites. In: Nixon, P. H. (ed.) *Mantle Xenoliths*. New York: John Wiley, pp. 537–550.

Dawson, J. B. (1984). Contrasting types of upper mantle metasomatism? The mantle and crust–mantle relationship. In: Kornprobst, J. (ed.) *Proceedings of the 3rd International Kimberlite Conference*. Amsterdam: Elsevier, pp. 289–294.

Dawson, J. B. (2004). A fertile harzburgite–garnet lherzolite transition: possible inferences for the roles of strain and metasomatism in upper mantle peridotites. *Lithos* **77**(1–4), 553–569.

Dawson, J. B. & Smith, J. V. (1975). Occurrence of diamond in a mica–garnet lherzolite xenolith from kimberlite. *Nature* **254**(5501), 580–581.

Dawson, J. B. & Smith, J. V. (1977). The MARID (mica–amphibole–rutile–ilmenite–diopside) suite of xenoliths in kimberlite. *Geochimica et Cosmochimica Acta* **41**(2), 309–310.

Dawson, J. B. & Smith, J. V. (1988). Metasomatized and veined upper-mantle xenoliths from Pello Hill, Tanzania—Evidence for anomalously ight mantle beneath the Tanzanian sector of the East African Rift Valley. *Contributions to Mineralogy and Petrology* **100**(4), 510–527.

Dawson, J. B. & Stephens, W. E. (1976). Statistical classification of garnets from kimberlite and associated xenoliths. *Journal of Geology* **53**, 589–607.

de Wit, M. J., de Ronde, C. E. J., Tredoux, M., Roering, C., Hart, R. J., Armstrong, R. A., Green, R. W. E., Peberdy, E. & Hart, R. A. (1992). Formation of an Archaean continent. *Nature* **357**(6379), 553–562.

Ekkerd, J., Stiefenhofer, J., Field, M. & Lawless, P. (2003). The geology of the Finsch Mine, Northern Cape Province, South Africa. In: *8th International Kimberlite Conference 8th International Kimberlite Conference Long Abstract*. Victoria, BC.

Finnerty, A. A. & Boyd, F. R. (1984). Evaluation of thermobarometers for garnet peridotites. *Geochimica et Cosmochimica Acta* **48**, 15–27.

Finnerty, A. A. & Boyd, F. R. (1987). Thermobarometry for garnet peridotites: basis for the determination of thermal and compositional structure of the upper mantle. In: Nixon, P. H. (ed.) *Mantle Xenoliths*. New York: John Wiley, pp. 381–402.

Fouch, M. J., James, D. E., VanDecar, J. C., van der Lee, S. & Kaapvaal Seismic Group (2004). Mantle seismic structure beneath the Kaapvaal and Zimbabwe Cratons. *South African Journal of Geology* **107**(1–2), 33–44.

Grégoire, M., Bell, D. R. & Le Roex, A. P. (2003). Garnet lherzolites from the Kaapvaal craton (South Africa): Trace element evidence for a metasomatic history. *Journal of Petrology* **44**(4), 629–657.

Griffin, W. L., Gurney, J. J. & Ryan, C. G. (1992). Variations in trapping temperatures and trace elements in peridotite-suite inclusions from African diamonds: evidence for two inclusion suites, and implications for lithosphere stratigraphy. *Contributions to Mineralogy and Petrology* **110**, 1–15.

Griffin, W. L., Fisher, N. I., Friedman, J., Ryan, C. G. & O'Reilly, S. Y. (1999*a*). Cr-pyrope garnets in the lithospheric mantle. I. Compositional systematics and relations to tectonic setting. *Journal of Petrology* **40**, 679–704.

Griffin, W. L., Shee, S. R., Ryan, C. G., Win, T. T. & Wyatt, B. A. (1999*b*). Harzburgite to lherzolite and back again: metasomatic processes in ultramafic xenoliths from the Wesselton kimberlite, Kimberley, South Africa. *Contributions to Mineralogy and Petrology* **134**(2–3), 232–250.

Griffin, W. L., O'Reilly, S. Y. & Ryan, C. G. (1999*c*). The composition and origin of subcontinental lithospheric mantle. In: Fei, Y., Bertka, C. M. & Mysen, B. O. (eds) *Mantle Petrology: Field Observations and High Pressure Experimentation: a Tribute to Francis R. (Joe) Boyd. Geochemical Society, Special Publications* **6**, 13–45.

Griffin, W. L., O'Reilly, S. Y., Natapov, L. M. & Ryan, C. G. (2003). The evolution of lithospheric mantle beneath the Kalahari Craton and its margins. *Lithos* **71**, 215–241.

Griffin, W. L., Graham, S., O'Reilly, S. Y. & Pearson, N. J. (2004). Lithosphere evolution beneath the Kaapvaal Craton: Re–Os systematics of sulfides in mantle-derived peridotites. *Chemical Geology* **208**(1–4), 89–118.

Grütter, H. S., Apter, D. B. & Kong, J. (1999). Crust–mantle coupling: evidence from mantle-derived xenocrystic garnets. In: Gurney, J. J., Gurney, J. L., Pascoe, M. D. & Richardson, S. H. (eds) *Proceedings of the 7th International Kimberlite Conference*. Cape Town: Red Roof Design, pp. 307–313.

Grütter, H., Latti, D. & Menzies, A. (2006). Cr-saturation arrays in concentrate garnet compositions from kimberlite and their use in mantle barometry. *Journal of Petrology* **47**(4), 801–820.

Grutzeck, M. W., Kridelbough, S. J. & Weill, D. F. (1974). The distribution of Sr and REE between diopside and the silicate liquid. *Geophysical Research Letters* **1**, 273–275.

Gurney, J. J. (1984). A correlation between garnets and diamonds. In: Glover, J. E. & Harris, P. G. (eds) *Kimberlite Occurrence and Origin: a Basis for Conceptual Models in Exploration*. Perth, Australia: University of Western, pp. 143–166.

Gurney, J. J. & Switzer, G. S. (1973). Discovery of garnets closely related to diamonds in Finsch Pipe, South Africa. *Contributions to Mineralogy and Petrology* **39**(2), 103–116.

Gurney, J. J., Harris, J. W. & Rickard, R. S. (1979). Silicate and oxide inclusions in diamonds from the Finsch kimberlite pipe.

In: Boyd, F. R. & Meyer, H. O. A. (eds) *Proceedings of the 2nd Kimberlite Conference. Geophysical Monograph, American Geophysical Union* **1**, 1–15.

Harte, B. (1977). Rock nomenclature with particular relation to deformation and recrystallisation textures in olivine-bearing xenoliths. *Journal of Geology* **85**, 297–288.

Hart, S. R. & Dunn, T. (1993). Experimental cpx/melt partitioning of 24 trace elements. *Contributions to Mineralogy and Petrology* **113**, 1–8.

Harte, B., Winterburn, P. A. & Gurney, J. J. (1987). Metasomatic phenomena in garnet peridotite facies mantle xenoliths from the Matsoku kimberlite pipe, Lesotho. In: Menzies, M. A. & Hawkesworth, C. J. (eds) *Mantle Metasomatism*. London: Academic Press, pp. 145–220.

Harte, B., Fitzsimons, I. C. W. & Kinny, P. D. (1996). Clinopyroxene–garnet trace element partition coefficients for mantle peridotite and melt assemblages. In: *V. M. Goldschmidt Conference Proceedings. Journal of Conference Abstracts* **1**, p. 235.

Hauri, E. H., Wagner, T. P. & Grove, T. L. (1994). Experimental and natural partitioning of Th, U, Pb and other trace elements between garnet, clinopyroxene and basaltic melts. *Chemical Geology* **117**, 149–166.

Hawkesworth, C. J., Erlank, A. J., Marsh, J. S., Menzies, M. A. & van Calsteren, P. (1983). Evolution of the continental lithosphere: evidence from volcanics and xenoliths in Southern Africa. In: Hawkesworth, C. J. & Norry, M. J. (eds) *Continental Basalts and Mantle Xenoliths*. Nantwich: Shiva, pp. 111–138.

Hervig, R. L., Smith, J. V., Steele, I. M. & Dawson, J. B. (1980). Fertile and barren Al–Cr-spinel harzburgites from the upper mantle: Ion and electron probe analyses of trace elements in olivine and orthopyroxene: Relation to lherzolites. *Earth and Planetary Science Letters* **50**(1), 41–58.

Herzberg, C. T. (1993). Lithosphere peridotites of the Kaapvaal craton. *Earth and Planetary Science Letters* **120**, 13–29.

Herzberg, C. (1999). Phase equilibrium constraints on the formation of cratonic mantle. In: Fei, Y., Bertka, C. M. & Mysen, B. O. (eds) *Mantle Petrology: Field Observations and High Pressure Experimentation: a Tribute to Francis R. (Joe) Boyd. Geochemical Society, Special Publications* **6**, 241–257.

Herzberg, C. (2004). Geodynamic information in peridotite petrology. *Journal of Petrology* **45**(12), 2507–2530.

Herzberg, C. & O'Hara, M. J. (2002). Plume-associated ultramafic magmas of Phanerozoic age. *Journal of Petrology* **43**(10), 1857–1883.

Hoal, K. E. O., Hoal, B. G., Erlank, A. J. & Shimizu, N. (1994). Metasomatism of the mantle lithosphere recorded by rare earth elements in garnets. *Earth and Planetary Science Letters* **126**(4), 303–313.

Ionov, D. A., Ashchepkov, I. V., Stosch, H. G., Witt-Eickschen, G. & Seck, H. A. (1993). Garnet peridotite xenoliths from the Vitim volcanic field, Baikal Region: the nature of the garnet–spinel peridotite transition zone in the continental mantle. *Journal of Petrology* **34**(6), 1141–1175.

James, D. E. & Fouch M. J. (2002). Formation and evolution of Archaean cratons: insights from southern Africa. In: Fowler, C. M. R., Ebinger, C.J. & Hawkesworth, C. J. (eds) *The Early Earth: Physical, Chemical and Biological Development. Geological Society, London, Special Publications* **199**, 1–26.

Jochum, K. P. (2006). MPI-DING reference glasses for *in situ* microanalysis: New reference values for element concentrations and isotope ratios. *Geochemistry, Geophysics, Geosystems* **7**, paper number Q02008.

Johnson, K. T. M., Dick, H. J. B. & Shimizu, N. (1990). Melting in the oceanic upper mantle: an ion microprobe study of diopsides in abyssal peridotites. *Journal of Geophysical Research* **95**, 2661–2678.

Jones, R. A. (1987). Strontium and neodymium isotopic and rare earth evidence for the genesis of megacrysts in kimberlites of southern Africa. In: Nixon, P. H. (ed.) *Mantle Xenoliths*. New York: John Wiley, pp. 711–724.

Kelemen, P. B., Hart, S. R. & Bernstein, S. (1998). Silica enrichment in the continental upper mantle via melt/rock reaction. *Earth and Planetary Science Letters* **164**(1–2), 387–406.

Kelley, S. P. & Wartho, J. A. (2000). Rapid kimberlite ascent and the significance of Ar–Ar ages in xenolith phlogopites. *Science* **289**(5479), 609–611.

Kennedy, C. & Kennedy, G. (1976). The equilibrium boundary between graphite and diamond. *Journal of Geophysical Research* **81**, 2467–2470.

Kesson, S. E. & Ringwood, A. E. (1989). Slab–mantle interactions. 2. The formation of diamonds. *Chemical Geology* **78**, 97–118.

Kinny, P. D. & Dawson, J. B. (1992). A mantle metasomatic injection event linked to late Cretaceous kimberlite magmatism. *Nature* **360**(6406), 726–728.

Kopylova, M. G. & Caro, G. (2004). Mantle xenoliths from the southeastern Slave craton: Evidence for chemical zonation in a thick, cold lithosphere. *Journal of Petrology* **45**(5), 1045–1067.

Li, A. & Burke, K. (2006). Upper mantle structure of southern Africa from Rayleigh wave tomography. *Journal of Geophysical Research* **111**(B10303), doi:10.1029/2006JB004321.

McDonough, W. & Sun, S.-s. (1995). The composition of the Earth. *Chemical Geology* **120**, 223–253.

McKenzie, D. & Bickle, M. J. (1989). The volume and composition of melt generated by extension of the lithosphere. *Journal of Petrology* **29**, 625–679.

McKenzie, D., Jackson, J. & Priestley, K. (2005). Thermal structure of oceanic and continental lithosphere. *Earth and Planetary Science Letters* **233**, 337–349.

Nair, S. K., Gao, S. S., Liu, K. H. & Silver, P. G. (2006). Southern African crustal evolution and composition: constraints from receiver function studies, *Journal of Geophysical Research*, **111**, B02304.

Nickel, K. G. (1989). Garnet–pyroxene equilibria in the system SMACCr (SiO_2–MgO–Al_2O_3–CaO–Cr_2O_3); the Cr geobarometer. In: Ross, J., Jaques, A. L. & Ferguson, J. *et al.* (eds) *Kimberlites and Related Rocks. Geological Society of Australia, Special Publications* **2**, 901–912.

Nixon, P. H., van Calsteren, P. W. C., Boyd, F. R. & Hawkesworth, C. J. (1987). Harzburgites with garnets of diamond facies from southern African kimberlites. In: Nixon, P. H. (ed.) *Mantle Xenoliths*. New York: John Wiley, pp. 523–534.

O'Neill, H. S. C. & Wood, B. J. (1979). An experimental study of Fe–Mg partitioning between garnet and olivine and its calibration as a geothermometer. *Contributions to Mineralogy and Petrology* **70**(1), 59–70.

Ono, S., Mibe, K. & Yoshino, T. (2002). Aqueous fluid connectivity in pyrope aggregates: water transport into the deep mantle by a subducted oceanic crust without any hydrous minerals. *Earth and Planetary Science Letters* **203**(3–4), 895–903.

O'Reilly, S., Griffin, W. L., Djomani, Y. & Morgan, P. (2001). Are lithospheres forever? *GSA Today* **11**, 4–10.

Pearce, N. J. G., Perkins, W. T., Westgate, J. A., Gorton, M. P., Jackson, S. E., Neal, C. R. & Chenery, S. P. (1997). A compilation of new and published major and trace element data for NIST SRM 610 and NIST SRM 612 glass reference materials. *Geostandards Newsletter* **21**, 115–144.

Pearson, D. G. (1999). The age of continental roots. *Lithos* **48**(1–4), 171–194.

Pearson, D. G., Boyd, F. R., Haggerty, S. E., Pasteris, J. D., Field, S. W., Nixon, P. H. & Pokhilenko, N. P. (1994). The characterisation and origin of graphite in cratonic lithospheric mantle: a petrological carbon isotope and Raman spectroscopic study. *Contributions to Mineralogy and Petrology* **115**, 449–466.

Pearson, D. G., Carlson, R. W., Shirey, S. B., Boyd, F. R. & Nixon, P. H. (1995*a*). The stabilisation of Archaean lithospheric mantle: a Re–Os isotope study of peridotite xenoliths from the Kaapvaal craton. *Earth and Planetary Science Letters* **134**, 341–357.

Pearson, D. G., Shirey, S. B., Carlson, R. W., Boyd, F. R., Pokhilenko, N. P. & Shimizu, N. (1995*b*). Re–Os, Sm–Nd, and Rb–Sr isotope evidence for thick Archaean lithospheric mantle beneath the Siberian craton modified by multistage metasomatism. *Geochimica et Cosmochimica Acta* **59**, 959–977.

Pearson, D. G., Irvine, G. J., Carlson, R. W., Kopylova, M. G. & Ionov, D. A. (2002). The development of lithospheric keels beneath the earliest continents: time constraints using PGE and Re-Os isotope systematics. *Geological Society, London, Special Publications* **199**, 65–90.

Pearson, D. G., Canil, D. & Shirey, S. B. (2003). Mantle samples included in volcanic rocks: xenoliths and diamonds. In: Holland, H. D. & Turekian, K. K. (eds) *Treatise on Geochemistry*. Amsterdam: Elsevier, pp. 171–275.

Pollack, H. N. & Chapman, D. S. (1977). On the regional variation of heat flow, geotherms, and lithospheric thickness. *Tectonophysics* **38**(3–4), 279–296.

Priestley, K. & McKenzie, D. (2006). The thermal structure of the lithosphere from shear wave velocities. *Earth and Planetary Science Letters* **244**, 285–301.

Richardson, S. H., Gurney, J. J., Erlank, A. J. & Harris, J. W. (1984). Origin of diamonds in old enriched mantle. *Nature* **310**(5974), 198–202.

Richardson, S. H., Shirey, S. B., Harris, J. W. & Carlson, R. W. (2001). Archean subduction recorded by Re–Os isotopes in eclogitic sulfide inclusions in Kimberley diamonds. *Earth and Planetary Science Letters* **191**(3–4), 257–266.

Richter, F. M. (1988). A major change in the thermal state of the Earth at the Archean–Proterozoic boundary: consequences for the nature and preservation of continental lithosphere. *Journal of Petrology, Special Lithosphere Volume* 39–52.

Rudnick, R. L., McDonough, W. F. & Orpin, A. (1994). Northern Tanzania peridotite xenoliths: a comparison with Kaapvaal xenoliths and inferences of metasomatic reactions. In: Meyer, H. O. A. & Leonardos, O. H. (eds) *Proceedings of the 5th International Kimberlite Conference*. Companhia de Pesquisa de Recursos Minerais **2**, pp. 336–353.

Ryan, C. G., Griffin, W. L. & Pearson, N. J. (1996). Garnet geotherms: Pressure–temperature data from Cr-pyrope garnet xenocrysts in volcanic rocks. *Journal of Geophysical Research* **101**(B3), 5611–5626.

Salters, V. J. M., Longhi, J. E. & Bizimis, M. (2002). Near mantle solidus trace element partitioning at pressures up to 3·4 GPa. *Geochemistry, Geophysics, Geosystems* **3**, doi:10.1029/2001GC000148.

Schmidberger, S. S. & Francis, D. (1999). Nature of the mantle roots beneath the North American craton: mantle xenolith evidence from Somerset Island kimberlites. *Lithos* **48**(1–4), 195 .

Schmitz, M. D., Bowring, S. A., de Wit, M. J. & Gartz, V. (2004). Subduction and terrane collision stabilize the western Kaapvaal craton tectosphere 2·9 billion years ago. *Earth and Planetary Science Letters* **222**(2), 363–376.

Schulze, D. (1991). Low Ca garnet harzburgite xenoliths from southern Africa: abundance composition and bearing on the structure and evolution of the subcratonic lithosphere. In: *5th International Kimberlite Conference, Extended Abstracts. CPRM Special Publication* **2**, 350–352.

Shee, S. R., Gurney, J. J. & Robinson, D. N. (1982). Two diamond-bearing peridotite xenoliths from the Finsch kimberlite, South Africa. *Contributions to Mineralogy and Petrology* **81**(2), 79–87.

Shimizu, N. & Richardson, S. H. (1987). Trace-element abundance patterns of garnet inclusions in peridotite-suite diamonds. *Geochimica et Cosmochimica Acta* **51**(3), 755–758.

Shimizu, N., Sobolev, N. V. & Yefimova, E. S. (1997). Chemical heterogeneities of inclusion garnets and juvenile character of peridotitic diamonds from Siberia. In: Dobrestov, N. L. (ed.) *Proceedings of the 6th International Kimberlite Conference. Russian Geology & Geophysics* **2**, 356–372.

Simon, N. S. C., Irvine, G. J., Davies, G. R., Pearson, D. G. & Carlson, R. W. (2003). The origin of garnet and clinopyroxene in 'depleted' Kaapvaal peridotites. *Lithos* **71**(2–4), 289–322.

Simon, N. S. C., Carlson, R. W., Pearson, D. G. & Davies, G. R. (2007). The origin and evolution of the Kaapvaal cratonic lithospheric mantle. *Journal of Petrology* **48**(3), 589–625.

Skinner, C. P. (1989). The petrology of xenoliths from the Finsch kimberlite. *South African Journal of Geology* **92**, 197–206.

Smith, C. B., Gurney, J. J., Skinner, E. M. W., Clement, C. R. & Ebrahim, N. (1985). Geochemical character of southern African kimberlites: a new approach based on isotopic constraints. *Transactions of the Geological Society of South Africa* **88**, 267–280.

Smith, C. B., Gurney, J. J., Harris, J. W., Otter, M. L., Kirkley, M. B. & Jagoutz, E. (1991). Neodymium and strontium isotope systematics of eclogite and websterite paragenesis inclusions from single diamonds, Finsch and Kimberley Pool, RSA. *Geochimica et Cosmochimica Acta* **55**(9), 2579–2590.

Smith, D. & Boyd, F. R. (1992). Compositional zonation in garnets in peridotite xenoliths. *Contributions to Mineralogy and Petrology* **112**(1), 134–147.

Sobolev, N. V., Pokhilenko, N. P. & Efimova, E. S. (1984). Xenoliths of diamond-bearing peridotites in kimberlites and the problem of diamond origin. *Geologia i Geofizica* **12**, 63–80.

Stachel, T. & Harris, J. W. (1997). Diamond precipitation and mantle metasomatism—evidence from the trace element chemistry of silicate inclusions in diamonds from Akwatia, Ghana. *Contributions to Mineralogy and Petrology* **129**(2), 143–154.

Stachel, T., Viljoen, K. S., Brey, G. & Harris, J. W. (1998). Metasomatic processes in lherzolitic and harzburgitic domains of diamondiferous lithospheric mantle: REE in garnets from xenoliths and inclusions in diamonds. *Earth and Planetary Science Letters* **159**(1–2), 1–12.

Stachel, T., Viljoen, K. S., McDade, P. & Harris, J. W. (2004). Diamondiferous lithospheric roots along the western margin of the Kalahari Craton—the peridotitic inclusion suite in diamonds from Orapa and Jwaneng. *Contributions to Mineralogy and Petrology* **147**(1), 32–47.

Stephens, W. E. & Dawson, J. B. (1977). Statistical comparison between pyroxenes from kimberlites and their associated xenoliths. *Journal of Geology* **85**, 433–449.

Tainton, K. M. & McKenzie, D. (1994). The generation of kimberlites, lamproites, and their source rocks. *Journal of Petrology* **35**(3), 787–817.

Thompson, R. N. & Gibson, S. A. (2000). Extremely magnesian olivines in Phanerozoic picrites signify transient high temperatures during mantle plume impact. *Nature* **407**, 502–506.

Tsai, H. M., Meyer, H. O. A., Moreau, J. & Milledge, H. J. (1979). Mineral inclusions in diamond: Premier, Jagersfontein and Finsch kimberlites, South Africa, and Williamson Mine, Tanzania. In: Meyer, H. O. A. & Boyd, F. R. (eds) *Proceedings of the 2nd Kimberlite Conference. Geophysical Monograph, American Geophysical Union* **1**, 16–26.

Tuff, J. & Gibson, S. A. (2007). Trace-element partitioning between garnet, clinopyroxene and Fe-rich picritic melts at 3 to 7 GPa. *Contributions to Mineralogy and Petrology* **153**(4), 369–387.

Van Orman, J. A., Grove, T. L., Shimizu, N. & Layne, G. D. (2002). Rare earth element diffusion in a natural pyrope single crystal at 2·8 GPa. *Contributions to Mineralogy and Petrology* **142**, 416–424.

Van Westrenen, W., Blundy, J. D. & Wood, B. J. (1999). Crystal-chemical controls on trace element partitioning between garnet and anhydrous silicate melts. *American Mineralogist* **84**, 838–847.

Van Westrenen, W., Blundy, J. D. & Wood, B. J. (2000). Effect of Fe^{2+} on garnet–melt trace element partitioning: Experiments in FCMAS and quantification of crystal-chemical controls in natural systems. *Lithos* **53**, 191–203.

Viljoen, K. S., Swash, P. M., Otter, M. L., Schulze, D. J. & Lawless, P. J. (1992). Diamondiferous garnet harzburgites from the Finsch Kimberlite, Northern Cape, South Africa. *Contributions to Mineralogy and Petrology* **110**(1), 133–138.

Viljoen, K. S., Robinson, D. N., Swash, P. M., Griffin, W. L., Otter, M. L., Ryan, C. G. & Win, T. T. (1994). Diamond- and graphite-bearing peridotite xenoliths from the Roberts Victor kimberlite, South Africa. In: Meyer, H. O. A. & Leonardos, O. H. (eds) *Kimberlites, Related Rocks and Mantle Xenoliths, Vol. 1. Proceedings of the Fifth International Kimberlite Conference. Companhia de Pesquisa de Recursos Minerais, Special Publication*, **1**, 285–303.

Walter, M. J. (1998). Melting of garnet peridotite and the origin of komatiite and depleted lithosphere. *Journal of Petrology* **39**(1), 29–60.

Wang, W., Sueno, S. & Takahashi, E. (1998). Influence of Cr on REE partitioning between garnet and silicate melt: application to metasomatism of mineral inclusions in diamonds. *Reviews of High Pressure Science and Technology* **7**, 92–94.

Wang, W., Sueno, S., Takahashi, E., Yurimoto, H. & Gasparik, T. (2000). Enrichment processes at the base of the Archean lithospheric mantle: observations from trace element characteristics of pyropic garnet inclusions in diamonds. *Contributions to Mineralogy and Petrology* **139**(6), 720–733.

Watson, E. B., Brenan, J. M. & Baker, D. R. (1990). Distribution of fluids in the continental mantle. In: Menzies, M. A. (ed.) *Continental Mantle*. Oxford: Clarendon Press, pp. 111–125.

Westerlund, K. J., Shirey, S. B., Richardson, S. H., Carlson, R. W., Gurney, J. J. & Harris, J. W. (2006). A subduction wedge origin for Paleoarchean peridotitic diamonds and harzburgites from the Panda kimberlite, Slave craton: evidence from Re–Os isotope systematics. *Contributions to Mineralogy and Petrology* **152**(3), 275–294.

Wood, B. J. & Blundy, J. (1997). A predictive model for rare earth element partitioning between clinopyroxene and anhydrous silicate melt. *Contributions to Mineralogy and Petrology* **129**, 166–181.

Wood, B. J. & Blundy, J. D. (2001). The effect of cation charge on crystal–melt partitioning of trace elements. *Earth and Planetary Science Letters* **188**(1–2), 59–71.

Xue, X., Baadsgaard, H., Irving, A. J. & Scarfe, C. M. (1990). Geochemical and isotopic characteristics of lithospheric mantle beneath West Kettle River, British Columbia: evidence from ultramafic xenoliths. *Journal of Geophysical Research* **95**, 15879–15891.